Patterns of morphological and molecular divergence of *Apodemus* (Rodentia: Muridae) species from the Western Palaearctic

Tina Klenovšek[1], Vida Jojić[2], Boris Kryštufek[3], Franc Janžekovič[4], Marko Djurakic[5]

[1]Faculty of Natural Sciences and Mathematics, University of Maribor, Slovenia
[2]Department of Genetic Research, Institute for Biological Research "Siniša Stanković" – National Institute of Republic of Serbia, University of Belgrade, Bulevar despota Stefana 142, 11060 Belgrade, Serbia
[3]Slovenian Museum of Natural History, Prešernova 20, 1000 Ljubljana, Slovenia
[4]Faculty of Natural Sciences and Mathematics, University of Maribor, Koroška cesta 160, 2000 Maribor, Slovenia
[5]Department of Biology and Ecology, Faculty of Sciences, University of Novi Sad, Trg Dositeja Obradovića 2, 21000 Novi Sad, Serbia

A - Research concept and design, B - Collection and/or assembly of data, C - Data analysis and interpretation, D - Writing the article, E - Critical revision of the article, F - Final approval of the article

Abstract:
Variation in the cranium, mandible, and upper molars across eight *Apodemus* species from the Western Palaearctic, *A. agrarius* (subgenus *Apodemus*), *A. alpicola*, *A. flavicollis*, *A. sylvaticus*, *A. uralensis*, *A*. *witherbyi* (subgenus *Sylvaemus*), and A. *epimelas* and *A*. *mystacinus* (subgenus *Karstomys*) is compared to molecular divergence. For the first time in this genus, molecular phylogeny is inferred from mitochondrial and nuclear loci using a multispecies coalescent approach. Also for the first time, all three structures are analysed using geometric morphometric methods within a single study and tested for the presence of phylogenetic signal. Our findings indicate that for each morphological structure analysed, *A. mystacinus* and *A. epimelas* have the highest mean centroid size values, whereas *A. uralensis* has the lowestsize variation among *Apodemus* species aligns with thermoregulatory expectations, although this remains a plausible rather than confirmed explanation due to the absence of direct test against temperature. The most distinctive mandible shapes are observed in *A. alpicola* and the subgenera *Apodemus* and *Karstomys*. *Karstomys* and *A. alpicola* also exhibit the most unique cranial morphology, while A. agrarius is characteriszed by its distinct molar shape. Phylogenetic signal is observed in the size and shape variation of each morphological structure analyszed, with the exception of cranial shape, supporting a mosaic model of morphological evolution in *Apodemus*. The subdivision into the three *Apodemus* subgenera is consistent only by molar shape, suggesting that molar morphology can serve as a reliable proxy for phylogenetic divergence and thus can be used to clarify phylogenetic relationships within the genus, particularly for fossil material where genetic data are unavailable.

Keywords: geometric morphometrics, mandible, molars, phylogenetic signal, cranium, multilocus phylogeny.

Received: 2025-07-11
Revised: 2026-01-03
Accepted: 2026-02-03
Final review: 2025-11-28

Short title
Morphological and molecular divergence in Apodemus

Corresponding author
Tina Klenovšek
Faculty of Natural Sciences and Mathematics, University of Maribor, Slovenia; email: tina.klenovsek@um.si

HYSTRIX
the Italian Journal of Mammalogy

ABSTRACT

Variation in the cranium, mandible, and upper molars across eight *Apodemus* species from the Western Palaearctic, *A. agrarius* (subgenus *Apodemus*), *A. alpicola*, *A. flavicollis*, *A. sylvaticus*, *A. uralensis*, *A. witherbyi* (subgenus *Sylvaemus*), and *A. epimelas* and *A. mystacinus* (subgenus *Karstomys*) is compared to molecular divergence. For the first time in this genus, molecular phylogeny is inferred from mitochondrial and nuclear loci using a multispecies coalescent approach. Also for the first time, all three structures are analysed using geometric morphometric methods within a single study and tested for the presence of phylogenetic signal. Our findings indicate that for each morphological structure analysed, *A. mystacinus* and *A. epimelas* have the highest mean centroid size values, whereas *A. uralensis* has the lowest. The most distinctive mandible shapes are observed in *A. alpicola* and the subgenera *Apodemus* and *Karstomys*. *Karstomys* and *A. alpicola* also exhibit the most unique cranial morphology, while *A. agrarius* is characterised by its distinct molar shape. Phylogenetic signal is observed in the size and shape variation of each morphological structure analysed, with the exception of cranial shape, supporting a mosaic model of morphological evolution in *Apodemus*. The subdivision into the three *Apodemus* subgenera is consistent only by molar shape, suggesting that molar morphology can serve as a reliable proxy for phylogenetic divergence and thus can be used to clarify phylogenetic relationships within the genus, particularly for fossil material where genetic data are unavailable.

Keywords: cranium; multilocus phylogeny; geometric morphometrics; mandible; molars; phylogenetic signal.

INTRODUCTION

Apodemus Kaup, 1829 is a genus of small rodents commonly known as field mice or wood mice. They belong to the family Muridae and are distributed primarily across temperate Europe, Asia, and parts of North Africa. The genus *Apodemus* comprises approx. 20 species, each with its specific distribution range and characteristics (Denys et al., 2017; Musser and Carleton, 2005). *Apodemus* is thought to be the oldest murine genus in Europe (Martín-Suárez and Mein, 1998), but the reconstruction of its ancient distribution revealed Western and Central Asia as the most likely centre of its origin (Ge et al., 2019). The genus has an extensive fossil history dating back to the Miocene and its emergence is placed in either the Early Vallesian (ca. 10–11.6 Mya; Martín-Suárez and Mein, 1998) or the Turolian (5.2–7 Mya; Schenk et al., 2013). The application of molecular clock dating estimated the most recent common ancestor of *Apodemus* at 6.4 Myr (Steppan and Schenk, 2017) or 9.84 Myr (Ge et al., 2019). Despite the fact that a sister genus of *Apodemus* is *Tokudaia* from the islands in the East China Sea (Steppan and Schenk, 2017) and basal species in the genus (*A. argenteus* and *A. gurka*) are entirely Asiatic, the Western Palaearctic region has been the stronghold for *Apodemus* since the Miocene, i.e. throughout the evolutionary history of the genus (Ge et al., 2019). In the W. Palaearctic, which includes Europe, North Africa and parts of the Middle East, ten *Apodemus* species are found (Burgin et al., 2020; Denys et al., 2017), which belong to three monophyletic groups that are usually ranked as distinct subgenera: *Apodemus* (*A. agrarius*), *Sylvaemus* (*A. alpicola*, *A. flavicollis*, *A. sylvaticus*, *A. uralensis*, *A. witherbyi*, *A. hyrcanicus* and *A. ponticus*) and *Karstomys* (*A. epimelas* and *A. mystacinus*). Eight of ten W. Palaearctic *Apodemus* species are endemic to the region, with the exception of *A. agrarius* and *A. uralensis*. The former is of Oriental origin and expanded into the W. Palaearctic after the Last Glacial Maximum (Yalkovskaya et al., 2022). The latter is distributed from central Europe to western China (Denys

et al., 2017) and belongs to a clade close to *A. flavicollis* (Darvish et al., 2015) or *A. flavicollis* + *A. alpicola* (Liu et al., 2012).

Over the past two decades, the use of genetic markers has substantially advanced our understanding of species diversity within the genus *Apodemus* (Mezhzherin and Tereshchenko, 2023; Ge et al., 2019; Balasanyan et al., 2018; Darvish et al., 2015; Kryštufek et al., 2012; Suzuki et al., 2008; Hoofer et al., 2007; Michaux et al., 2002). Analyses based on mitochondrial markers (cytochrome *b* and *12S rRNA*) and a nuclear marker (*IRBP*) have revealed three deeply divergent lineages corresponding to the subgenera *Apodemus*, *Sylvaemus*, and *Karstomys* (Michaux et al., 2002). In the case of W. Palaearctic species, subsequent studies, predominantly based on cytochrome *b*, have provided two key insights. First, they revealed multiple distinct clades within nominal species of *Sylvaemus*, indicating substantial unrecognized diversity and complex evolutionary histories in *A. sylvaticus* (Herman et al., 2017; Michaux et al., 2003), *A. flavicollis* (Yalkovskaya et al., 2018; Michaux et al., 2004), *A. mystacinus* (Olgun Karacan, 2023; Michaux et al., 2005), *A. uralensis* (Balasanyan et al., 2018; Chelomina and Atopkin, 2010), *A. witherbyi* (Balasanyan et al., 2018), and *A. agrarius* (Latinne et al., 2020). Second, they prompted taxonomic revisions of some morphologically identified specimens (Kryštufek et al., 2012, see our Supplementary material S1 and Supplementary Fig. S1). While cytochrome *b* remains a widely used marker in *Apodemus* phylogenetics, it has notable limitations that complicate comparisons across studies. These include variation in sampling strategies, methodological differences in phylogenetic inference, and the presence of nuclear mitochondrial pseudogenes (numts) in some specimens (Dubey et al., 2009). Additionally, cytochrome *b* is prone to saturation at third codon positions, which can obscure deeper phylogenetic signals (Suzuki et al., 2008; Michaux et al., 2002). These challenges highlight the importance of

cautious interpretation and the need for multilocus approaches incorporating nuclear markers to clarify species boundaries and evolutionary relationships within *Sylvaemus*.

Interspecific morphological divergence in *Apodemus* has been studied in the context of taxonomy (Helvaci and Çolak, 2021; Okulova et al., 2019; Darvish et al., 2014; Jojić et al., 2012; Barčiová and Macholán, 2009; Kryštufek and Vohralík, 2009; Kuncová and Frynta, 2009; Çolak et al., 2007; Frynta et al., 2006; Janžekovič and Kryštufek, 2004) or ecology (Kerr et al., 2017; Renaud and Michaux, 2003). More rarely, molecular and morphological divergence have been contrasted to assess the correspondence or lack of it (Ge et al., 2019; Çolak et al., 2007; Frynta et al., 2006; Renaud and Michaux, 2003; Hille et al., 2002). Traditionally, most studies on the morphological variability of *Apodemus* (Ge et al., 2019; Okulova et al., 2019; Knitlova and Horaček, 2017; Darvish et al., 2014; Barčiová and Macholán, 2009; Kryštufek and Vohralík, 2009; Kuncová and Frynta, 2009; Çolak et al., 2007; Frynta et al., 2006; Hille et al., 2002; Filippucci et al., 1996; Musser et al., 1996) have used craniodental and/or body linear measurements as morphological characters. Such measurements, some of which are also diagnostic in species taxonomy, provide valuable and comparable results, but fail to recover the shape of the original form as they do not capture the geometrical relationships among the measurements (Rohlf and Marcus, 1993). Alternatively, Fourier methods have been used in outline analyses of *Apodemus* molars (Helvaci and Çolak, 2021; Ledevin et al., 2012) and mandibles (Ledevin et al., 2012; Renaud et al., 2007; Renaud and Michaux, 2003). Despite well-established landmark-based geometric morphometric methods (Rohlf and Slice, 1990) that can, among others, capture and preserve the geometry of complex structures throughout analyses, separate size and shape data, and provide powerful visualizations of even very subtle shape changes for various research purposes (Klingenberg, 2013), only few studies employed it on

Apodemus, either for a single one or up to two skeletal elements within the same study (upper molars: Janžekovič and Kryštufek, 2004; cranium: Dúhová, 2020; cranium and mandible: Jojić et al., 2012). Different skeletal elements may evolve at different rates and follow different developmental pathways, respond to different selection pressures due to functional constraints, and be exposed to different environmental influences, i.e. their genetics, development and function differ in ways that could influence their adaptive responses (Caumul and Polly, 2005), not ignoring the role of genetic drift in their evolution (Felsenstein, 2002). All this combined may lead to different degrees of similarity between the divergence of a particular morphological character and the phylogenetic structuring of taxa (Kryštufek et al., 2016; Lu et al., 2014; Ledevin et al., 2012; Caumul and Polly, 2005). In *Apodemus*, the shape of the three most frequently studied structures – cranium, mandible and molars, gave mixed results, either showing good (cranium: Dúhová, 2020; Frynta et al., 2006; mandible: Renaud et al., 2007; molars: Helvaci and Çolak, 2021; Ledevin et al., 2012) or poor (mandible: Ledevin et al., 2012; Renaud and Michaux, 2003) agreement between the phenetic relationships and the phylogeny. In general, good agreement was more frequent, but it must be noted that poor agreement could be underreported due to publication bias, selective reporting or favouring of positive results. Also, the results cannot be directly compared because of differences in morphometric methods and taxonomic sampling. Moreover, the phylogenetic reconstruction of the genus, which was used for comparison with morphology, has changed over the past decades.

In this study, we investigated the phylogenetic relationships among W. Palaearctic *Apodemus* species using published sequences from four mitochondrial loci (cytochrome *b*, *12S rRNA*, D-loop, *COI*) and four nuclear loci (*IRBP*, *RAG1*, *I7*, *vWF*). For the first time in this group, we applied a multispecies coalescent (MSC) framework based on multilocus data

(Douglas et al., 2022; Liu et al., 2009) to infer evolutionary history. Complementing the molecular analysis, we conducted two-dimensional geometric morphometric analyses on three key cranial structures, mandible, cranium, and upper molars, widely used in studies of small mammal morphology. This integrative approach enabled us to evaluate the relative contributions of phylogenetic signal and adaptive processes to morphological variation within the genus. We defined two main objectives: (1) to assess whether any of the examined morphological structures can reliably reflect phylogenetic relationships and thus aid in resolving taxonomic uncertainties within *Apodemus*, and (2) to explore how adaptive processes influence cranial morphology, particularly identifying which regions of the skull are most affected. To this end, we analysed ten populations representing eight *Apodemus* species from the W. Palaearctic. Phenetic relationships were inferred from patterns of size and shape variation in the cranium, mandible, and molars, and interpreted in light of molecular phylogeny. Notably, this is the first study to apply geometric morphometric methods to all three major cranial structures within a single comparative framework across a broad sampling of *Apodemus* species from the W. Palaearctic.

MATERIAL AND METHODS

Sample for morphometric analyses

The analysed sample included 264 mandibles, 275 crania, and 286 upper molars from eight *Apodemus* species from the Western Palearctic: *A. agrarius*, *A. alpicola*, *A. flavicollis*, *A. sylvaticus*, *A. uralensis*, *A. witherbyi*, *A. epimelas*, and *A. mystacinus* (Table 1). As some mandibles and/or crania were damaged, there were 230 specimens (80.4% of the total) in which all three structures (mandible, cranium and molars) were used. Two species were represented by geographically distinct populations, *A. flavicollis* from Slovenia and Anatolian Turkey, and *A. uralensis* from the Czech Republic and Anatolian Turkey. Altogether ten OUTs were considered in morphometric analyses. In analyses of the phylogenetic signal in morphometric data, we treated the two populations of *A. flavicollis* as separate taxa, and the sample of *A. uralensis* as a single taxon (see justification in Supplementary Figs. S1, S2 and Results related to the Phylogenetic reconstruction and divergence dating). Only adult specimens with fully erupted permanent dentition were studied, originating from the collections of the Slovenian Museum of Natural History (Ljubljana, Slovenia), the Natural History Museum Vienna (Vienna, Austria) and the Institute of Vertebrate Biology (Brno, Czech Republic).

Vouchers of the closely resembling species, *A. flavicollis* and *A. sylvaticus*, were captured in regions where only a single *Apodemus* species occurs, with their identities verified in other studies. Additional morphometric comparison of *A. flavicollis* and *A. sylvaticus* cranial data is presented in the Morphometric data acquisition and morphometric analysis.

Sample for molecular phylogenetic reconstruction

To reconstruct the phylogenetic relationships among *Apodemus* species in line with the morphological sampling scheme, we first assessed whether geographically distant populations of both *A. flavicollis* (including specimens genetically related to *A. ponticus*) and *A. uralensis* should be considered separate evolutionary lineages in the MSC. This evaluation was based on cytochrome *b* sequences, the most widely represented mitochondrial marker for these taxa in GenBank, with broad geographic coverage. The cytochrome *b* dataset comprised 317 sequences for *A. flavicollis* and *A. ponticus*, and 131 sequences for *A. uralensis* (Supplementary material S1). Sixteen cytochrome *b* sequences (15 *A. witherbyi* (reported as *A. fulvipectus*) and 1 *A. sylvaticus*) were used as outgroups in analyses of the *A. flavicollis–ponticus* group, while a single *A. sylvaticus* sequence was used as an outgroup for *A. uralensis* (Supplementary material S1).

For the MSC, we included 48 individuals representing nine *Apodemus* species (*A. flavicollis*: 6, *A. ponticus*: 3, *A. sylvaticus*: 5, *A. uralensis*: 6, *A. alpicola*: 5, *A. witherbyi*: 5, *A. epimelas*: 5, *A. mystacinus*: 8, *A. agrarius*: 5), and six outgroup individuals (*Tokudaia osimensis*: 2, *Malacomys longipes*: 4). From these 54 specimens, we included 160 sequences for eight loci, obtained from GenBank and originating from previously published studies (Supplementary material S2): four mitochondrial loci (cytochrome *b*, *12S rRNA*, D-loop, *COI*) and four nuclear loci (*IRBP*, *RAG1*, *I7*, *vWF*). No individual was represented at all eight loci. Gene coverage per specimen ranged from 12.5% (1 of 8 loci) to 62.5% (5 of 8 loci), with an average coverage of 37% (3 of 8 loci) across the 54 individuals (Supplementary material S2). To retain the full extent of available data, we chose not to concatenate sequences from different individuals, but instead retained the sparse data matrix in the MSC framework. Concatenated sequence approach appeared to bias the estimate of branch lengths, substitution rates and yield to inconsistent tree

typologies (Douglas et al., 2022). Likewise, the MSC analysis is robust and can successfully handle missing data (Jordan Douglas, personal communication).

Phylogenetic analysis and divergence dating

Multiple sequence alignment for each gene was performed in AliView (version 1.30) (Larsson, 2014) which uses Muscle (version 3.8.425) (Edgar, 2004). To test if geographically distant populations of both *A. flavicollis* (333 sequences, trimmed alignment of 969bp, Supplementary material S1) and *A. uralensis* (132 sequences, trimmed alignment of 1014bp, Supplementary material S1) should be considered separate evolutionary lineages as well to provide justification for sequences grouping scheme required for MSC, we perform maximum likelihood phylogenetic reconstruction in IQ-TREE (version 3.0.1) (Wong et al., 2025) using default settings and ultrafast bootstrap approximation (Hoang et al., 2018) via online web platform (http://iqtree.cibiv.univie.ac.at/).

In MSC analysis eight loci alignments (cytochrome *b*: 970bp, *12S rRNA*: 981bp, D-loop: 1163bp, *COI*: 719bp, *IRBP*: 1205bp, *RAG1*: 1002bp, *I7*: 792bp, *vWF*: 1191bp) from 54 individuals were grouped into 11 species (nine *Apodemus spp.* + two outgroup species, Supplementary material S2) and dated phylogenetic relationship was estimated in StarBeast3 package (version 1.1.9) (Douglas et al., 2022) for BEAST 2 (version 2.7.7) (Bouckaert et al., 2019). The input parameters for BEAST 2 were set as follows. Site model, clock model and trees were treated independent (unlinked) for all loci during estimation of relative rates of substitution among branches, tree topology and branching times. Gene ploidy for mitochondrial and nuclear loci was set to 0.5 and 2, respectively. For each locus a site model and associated substitution model were estimated with bModelTest (version 1.3.3) (Bouckaert and Drummond, 2017) using

transition and transversion prior model through MCMC. Gene clock model was estimated for all loci except cytochrome *b* which was fixed at 1. Species tree was estimated under relaxed clock model where both mean clock rate and standard deviation were estimated with log normal prior where M and S were initially set to 0.001 and 0.1, respectively, in real space. Because we used node calibration during analysis, calibrated Yule model was used with speciation rate prior under the log normal distribution with M and S parameters set to 0.16 and 0.4, respectively, in real space. The node of the most recent common ancestor of Apodemini tribus (*Tokudaia* and *Apodemus* genera) was calibrated using log normal distribution prior (M=0.6, S=0.7 in real space, offset=10.1) which place their split about 10.7 Mya (Kimura et al., 2017). Likewise, the split between *Apodemus* and (*Karstomys* + *Sylvaemus*) was approximated with normal distribution (mean=7, sigma=1.1) (Michaux et al., 2005, 2002). The posterior distribution of parameters were estimated with MCMC sampling where samples dawn every 100 000 steps over 20 000 000 iterations. We ran two chains and discarded 10% of the sample via burn-in. A convergence of estimated parameters was tested in Tracer (version 1.7) (Rambaut et al., 2018). All parameters reached considerably over recommended 200 ESS values except TreeDistanceUPGMA.t:cyt_b, BMT_gamaShape.s:coi_site, hasGammaRates.s:coi_site, ActiveProportionInvariable.s:coi_site and cySpeciationRate.t:Species which did not affect the topology of the maximum clade credibility tree (results not shown). We also run BEAST 2 MCMC by sampling just from a prior in order to check the distribution of parameters of the model without the data. Afterwards, TreeAnnotator (version 2.7.4) was utilized to summarize the information from a sample of trees produced by BEAST 2 and the maximum clade credibility tree where node heights were expressed as median heights was calculated and visualized via IcyTree (Vaughan, 2017) online platform. The maximum clade credibility tree was used as input

tree file in subsequent comparative geometric morphometric analysis in MorphoJ v. 1.07a (Klingenberg, 2011).

Morphometric data acquisition and morphometric analysis

Two-dimensional landmarks were recorded on images (Fig. 1) of the mandible in labial view (12 landmarks), the cranium in ventral view (16 landmarks), and the maxillary molars in occlusal view (14 landmarks) using tpsDig software (Rohlf, 2015a, b).

Size and shape variation of the mandible, crania, and the upper molars were studied separately using geometric morphometric methods based on Procrustes superimposed landmarks (Dryden and Mardia, 1998; Rohlf and Marcus, 1993; Bookstein, 1991). To extract information on variation in size (centroid size, CS) and shape (Procrustes coordinates) from the landmark data, the raw landmark coordinates of all specimens belonging to ten operational taxonomic units (OTUs) of *Apodemus* (Table 1) were superimposed using Generalized Procrustes Analysis (GPA) (Rohlf, 1999; Dryden and Mardia, 1998; Rohlf and Slice, 1990).

To confirm the identification of specimens of phenotypically similar OTUs (*A. flavicollis* SI and *A. sylvaticus*; although the latter is smaller), we used cranial data and performed two Principal Component Analyses (PCAs): the first using the covariance matrix of Procrustes coordinates, and the second based on the covariance matrix of residuals from a multivariate regression of Procrustes coordinates onto log-transformed centroid size (log CS). We also conducted two multivariate analyses of variance (MANOVAs): the first using Procrustes coordinates, and the second using residuals from the multivariate regression of Procrustes coordinates onto log CS as the dependent variables, with OTU as the independent variable. Results (not shown) indicated clear separation of the two OTUs in PCA ordination space and

statistically significant difference (MANOVA), with cranial differences between *A. flavicollis* and *A. sylvaticus* consistent with those previously observed by both traditional morphometrics (Kryštufek and Stojanovski, 1996; Tvrtković, 1979; Niethammer, 1969) and geometric morphometrics (Jojić et al., 2014).

To estimate sexual size and shape dimorphism in the mandibles, crania, and upper molars within each OTU, except those with high numbers of individuals of unknown sex (*A. agrarius*, *A. flavicollis* SI, *A. sylvaticus*, and *A. epimelas*; Table 1), we regressed CS and Procrustes coordinates onto the sex dummy variables. We observed statistically insignificant sexual size and shape dimorphism in all three morphological structures (results not shown) within each OTU (*A. alpicola*, *A. flavicollis* TR, *A. uralensis* CZ, *A. uralensis* TR, *A. witherbyi* and *A. mystacinus*). Likewise, previous study reported no sexual size dimorphism in the mandibles, crania, and the upper molars of *A. agrarius*, *A. alpicola*, *A. flavicollis*, *A. sylvaticus*, *A. uralensis*, and *A. epimelas* (Janžekovič and Kryštufek, 2004). Jojić et al. (2012) also provided evidence of no sexual size dimorphism in the mandibles and crania of *A. agrarius*, *A. flavicollis*, *A. sylvaticus* and *A. epimelas*, as well as no sexual shape dimorphism in the crania, while sexual differences in mandibular shape within these four species were smaller than shape differences between species. Therefore, in the subsequent analyses we included specimens of unknown sex and pooled the sexes.

To examine size variation, we conducted an analysis of variance (ANOVA) with CS as the dependent variable and OTU as the independent variable. We also performed the pairwise post-hoc tests for all OTUs as a series of regressions of CS on dummy variables for pairs of OTUs. The statistical significance of size differences between the analysed OTUs was evaluated

using a permutation test with 10,000 permutation runs (Edgington, 1995; Good, 1994). Finally, we plotted the means, standard deviations, and standard errors of CS for the OTUs analysed.

To examine shape variation, we first performed MANOVA with Procrustes coordinates as the dependent variables and OTU as the independent variable. Then, we conducted the pairwise permutation tests (with 10,000 permutation runs) for all OTUs as a series of regressions of Procrustes coordinates on dummy variables for pairs of OTUs. Classification accuracy of OTUs was assessed by applying a leave-one-out cross-validated Discriminant Function Analysis (DFA) (Lachenbruch, 1967). To visually examine patterns of shape variation, we applied Canonical Variate Analysis (CVA). Warped outline drawings (Klingenberg, 2013) were used to visually identify the extent and direction of shape variation between OTUs separated along the CV axes.

(M)ANOVA and leave-one-out cross-validated DFA were performed in SPSS v. 25.0 (IBM Corp, 2017). All other analyses were done in MorphoJ v. 1.07a (Klingenberg, 2011).

Analysis of the phylogenetic signal in morphometric data

To test for the presence of a phylogenetic signal in the morphometric data, we mapped the geometric morphometric data to a phylogeny using weighted squared-change parsimony (Klingenberg and Gidaszewski, 2010). To test whether the pattern of morphological (mandibular, cranial, and upper molar) size and shape variation reflects the phylogenetic pattern, a permutation test (with 10,000 iterations) was performed against the null hypothesis of the absence of phylogenetic structure in the morphometric data. We also superimposed the phylogeny onto the morphospace defined by the first two principal components (PCs) of the covariance matrix among the average shapes of the analysed OTUs (Klingenberg and Gidaszewski,

2010). MorphoJ v. 1.07a (Klingenberg, 2011) was used for these analyses. Finally, we assessed congruence between the MSC phylogeny and UPGMA phenograms derived from Procrustes distance matrices among mean OTU shapes using a co-phylogenetic tree comparison implemented in cophylo (phytools v.2.4-4; Revell, 2024). The MSC tree was converted to class "phylo" and pruned of outgroups. For each morphological structure, UPGMA phenograms were generated with hclust in base R and converted to "phylo" objects. Trees were compared using cophylo with rotate = TRUE to optimize vertical correspondence of nodes. Shape variation for each OTU was mapped onto terminal branches of the UPGMA phenograms as deviations from the grand mean shape.

RESULTS

Phylogenetic reconstruction and divergence dating

The phylogenetic inference of 317 cytochrome *b* sequences of *A. flavicollis* sensu lato via maximum likelihood analysis showed two clear, deep, well supported geographically segregated genetic lineages (Supplementary Fig. S1). For instance, all European samples (including the European part of Turkey - Thrace), part of Russian samples (Urals, Samara, Volgograd, Voronezh) and Kazahstan form a lineage that we annotated as *A. flavicollis* SI (abbreviation for Slovenia). Samples from Georgia, Iran, Israel, the Anatolian part of Turkey and single Russian sample (Krasnodar) form a lineage annotated as *A. flavicollis* TR (abbreviation for Turkey (Türkiye)). The only exception is single sample from north-east part of Turkey (Damar, AJ605666) which group within *A. flavicollis* TR clade. Altogether, we treat *A. flavicollis* lineages as two separate species in the following MSC analysis. In contrast to *A. flavicollis* sensu

lato, the phylogenetic inference of 131 cytochrome *b* sequences of *A. uralensis* didn't show clear geographical segregation (Supplementary Fig. S2). Although samples from Czech Republic and Anatolia genetically differed to some extent, we didn't observe well supported split via ultrafast bootstrap methods in our maximum likelihood analysis. Therefore, due to unclear geographic clustering of the sequences, we treat *A. uralensis* as single species in MSC.

The phylogenetic relationships among the 11 taxa were estimated using a time-calibrated MSC model and these relationships are summarized in Fig. 2 as a maximum clade credibility tree, showing posterior median divergence times and posterior probabilities (pp) for each node. The split between the Apodemini tribe (*Tokudaia* and *Apodemus* genera) and *Malacomys longipes* (tribe Malacomyini) is estimated at approximately 11.2 Mya (95% HPD: 10.3–12.9), while within Apodemini, the divergence between *Tokudaia* and *Apodemus* occurred around 10.6 Mya (95% HPD: 10.2–11.6). Both nodes are strongly supported (pp=1.0).

Within the *Apodemus* genus, the split between *A. agrarius* (subgenus *Apodemus*) and the clade comprising subgenera *Karstomys* and *Sylvaemus* occurred approximately 9.76 Mya (95% HPD: 7.7–10.9), though this node is only moderately supported (pp=0.63). The divergence between *Karstomys* and *Sylvaemus* is estimated at 7.37 Mya (95% HPD: 5.86–8.73), with strong support (pp=1.0). Within *Karstomys*, *A. epimelas* and *A. mystacinus* diverged around 1.57 Mya (95% HPD: 0.43–3.66), also with high support (pp=1.0).

Within *Sylvaemus*, the earliest divergence separates *A. witherbyi* from all other members, dated to approximately 3.88 Mya (95% HPD: 2.91–5.16; pp=1.0). This is followed by the divergence of *A. uralensis* from the remaining *Sylvaemus* taxa around 2.70 Mya (95% HPD: 1.98–3.81; pp=0.99). Subsequently, *A. alpicola* diverged from the clade containing *A. flavicollis*

sensu lato at about 1.93 Mya (95% HPD: 1.21–2.79; pp=0.98), with the final split between the *A. flavicollis* SI and TR lineages estimated at 1.36 Mya (95% HPD: 0.42–2.24; pp=0.8).

Size variation

Analyses of variance (ANOVAs) for centroid size disclose significant size differences among *Apodemus* OTUs (mandible: $F_{9,254}$=149.08, *P*=0.0000, *Rsq*=0.8408; cranium: $F_{9,265}$=240.77, *P*=0.0000, *Rsq*=0.8910; molars: $F_{9,276}$=388.06, *P*=0.0000, *Rsq*=0.9268). The results of the pairwise *Apodemus* OTUs comparisons are shown in Supplementary Table S1. The majority of pairwise comparisons reveal statistically significant (*P*<0.001 after Bonferroni correction) size differences between *Apodemus* OTUs. The average *Rsq* is the highest (63.3%) for molars, followed by that for cranium (55.5%), and the lowest for mandible (53.4%). The plots of the means of the centroid sizes, standard deviations, and standard errors for the *Apodemus* OTUs are given in Supplementary Fig. S3. *Apodemus mystacinus* and *A. epimelas* have the highest centroid size mean values, whereas *A. uralensis* from the Czech Republic and Turkey have the smallest. Although *A. epimelas* differs the most from the other OTUs (Supplementary Table S1), *A. mystacinus* has the largest mandibles, crania and molars, while *A. uralensis* from the Czech Republic the smallest (Supplementary Fig. S3). All OTU pairs containing *A. uralensis* from the Czech Republic and Turkey differ significantly in mandibular size. In terms of variation in cranial size, all OTU pairs comprising *A. epimelas*, *A. mystacinus* and *A. uralensis* from the Czech Republic differ significantly. In the variation of molar size, only OTU pairs containing *A. flavicollis* from Slovenia are significantly different (Supplementary Table S1).

Shape variation

Multivariate analyses of variance (MANOVAs) reveal significant shape differences among *Apodemus* OTUs (mandible: λWilks=0.0009, $F_{180,1956.94}$=14.65, P=0.0000; cranium: λWilks=0.0002, $F_{252,2066.18}$=14.35, P=0.0000; molars: λWilks=0.0028, $F_{216,2159.97}$=10.04, P=0.0000). All *Apodemus* OTU pairs differ significantly (P<0.001 after Bonferroni correction) in the shape variation of the analysed morphological structures, except for *A. witherbyi* and *A. uralensis* from Turkey in the variation of the cranial shape (Supplementary Table S2). The average *Rsq* value is the highest (26.8%) for the cranium, followed by that for the mandible (26.6%) and the lowest for the molars (19.2%). According to the average *Rsq* values, *A. mystacinus* differs the most for mandibular shape variation, *A. epimelas* for cranial and *A. agrarius* for molar.

The classification accuracies of the OTUs assessed by the application of leave-one-out cross-validated Discriminant Function Analysis (DFA) for mandible, cranium and upper molars are shown in Tables 2–4. Cross-validated DFAs reveal that 81.4% of the mandibles, 80.7% of the crania, and 70.3% of the molars are correctly reclassified.

Mandibular shape variation

Canonical Variate Analysis (CVA; Fig. 3) separates members of the subgenus *Karstomys* (*A. epimelas* and *A. mystacinus*) from members of the other two subgenera along the CV1 axis, and differences are the most pronounced between *A. mystacinus* and *A. alpicola*. The CV2 axis separates *A. mystacinus* (subgenus *Karstomys*), *A. agrarius* (subgenus *Apodemus*) and *A. alpicola* (subgenus *Sylvaemus*) from the others, and differences in mean mandibular shape along the CV2 axis are the most pronounced between *A. alpicola* and *A. sylvaticus*. Changes in mandibular shape along the CV1 axis are evident throughout the structure. In the posterior part of the mandible (ascending ramus), members of the subgenus *Karstomys* are characterised by the larger condylar and angular but smaller coronoid processes compared to the other two subgenera. In the anterior part of the mandible (alveolar region), the mice of the subgenus *Karstomys* have a slightly longer molar row in the region of the first molar and more robust zones of molar and incisor alveoli with an anterior shortening of the mandible (shorter diastema) compared to the other subgenera. Shape changes along the CV2 axis are visible throughout the mandible. Compared to other species, *A. mystacinus*, *A. agrarius*, and *A. alpicola* generally have lower mandibles with elongation of the region between the condylar and angular processes and the incisor alveolus. In addition, their mandibles are characterised by a larger mandibular notch (i.e. shortened and anteriorly directed coronoid process).

Cranial shape variation

Canonical Variate Analysis (CVA; Fig. 4) – CV1 axis separates *A. epimelas* and *A. mystacinus* (subgenus *Karstomys*) and *A. alpicola* (subgenus *Sylvaemus*) from *A. agrarius* (subgenus *Apodemus*) and other members of subgenus *Sylvaemus*. Differences in mean cranial shape along the CV1 axis are most pronounced between *A. epimelas* and *A. agrarius*. The CV2 axis separates *A. alpicola* from other OTUs. Differences in mean cranial shape along the CV2 axis are the most pronounced between *A. alpicola* and *A. epimelas* and *A. sylvaticus* The changes in cranial shape along the CV1 axis encompass the entire structure. Compared to other species, *A. epimelas*, *A. mystacinus* and *A. alpicola* have slimmer crania with more compressed basicrania. They also have a longer *foramen incisivum*, a slightly smaller *bulla tympanica*, and diverged zygomatic arches. Shape variation along the CV2 axis is visible throughout the cranium. Compared to other species, *A. alpicola* has a narrower cranium with longer rostrum and compressed basicranium, somewhat shorter *foramen incisivum*, and smaller *bulla tympanicum*.

Upper molar shape variation

Canonical Variate Analysis (CVA; Fig. 5) – CV1 axis separates members of the subgenera *Sylvaemus* and *Karstomys* from *A. agrarius* (subgenus *Apodemus*). Differences in mean molar shape along the CV1 axis are most pronounced between *A. alpicola* and *A. agrarius*. Changes in molar shape along the CV1 axis are generally in the labial-lingual direction and include all three molars. Compared to subgenera *Sylvaemus* and *Sylvaemus*, species of the subgenus *Apodemus* (*A. agrarius*) is characterised by less robust molars with the first molar being particularly long. The CV2 axis separates *A. agrarius* from *A. epimelas* and *A. mystacinus*, and molar shape differences along the CV2 axis are most pronounced between *A. agrarius* and *A. epimelas*. Shape changes along the CV2 axis are distributed across the entire molar row. Compared to *A. epimelas*, *A. agrarius* has a narrower and longer molar row.

Phylogenetic signal in size and shape variation

A phylogenetic signal in size variation is observed for all morphological structures studied, while the presence of a phylogenetic signal in shape variation is noted for the mandible and upper molars. For the cranium, the permutation test shows the absence of a phylogenetic structure in shape variation (Table 5). Phylo-PCA plots of mean shapes for the analysed *Apodemus* OTUs (Supplementary Fig. S4) showed OTU distributions comparable to those in the CVA plots (Figs. 3-5). Similarly, shape changes associated with the first two PCs are similar to those of the CVA and are therefore not presented. Unlike the phylo-PCA plots for mandibular and molar shape, the projection of the phylogenetic tree into the PC plot for cranial shape revealed a long branch between the related *Apodemus* species (*A. epimelas* and *A. mystacinus*)

and a crossing of the *A. agrarius* branch, confirming the absence of phylogenetic structure in the cranial shape variation (Supplementary Fig. S4). Co-phylogenetic plots comparing the reconstructed MSC phylogeny with mandibular, cranial, and molar UPGMA phenograms, annotated with OTU mean shapes relative to the grand mean, are shown in Figs. 6–8. Correspondence between the MSC phylogeny and UPGMA phenograms was lowest for cranial shape and highest for molar shape. The molar UPGMA largely recovered the subgeneric clustering observed in the MSC phylogeny, except for species within *Sylvaemus*, which remained incongruent with relationships inferred from molecular data. Phylogenetic signal was detected only in mandible and molar shape data (Figs. 6 and 8).

DISCUSSION

Molecular divergence

This study provides the first phylogeny of Western Palaearctic *Apodemus* species inferred under the multispecies, multilocus coalescent (MSC) model (Douglas et al., 2022; Liu et al., 2009) using exclusively published sequences. The MSC framework, which jointly estimates gene and species trees within a Bayesian framework, is particularly suitable for resolving recent evolutionary events and accounting for incomplete lineage sorting, processes suspected in *Apodemus* (e.g., Suzuki et al., 2008; Michaux et al., 2002).

Our reconstructed phylogeny supports the division of the genus *Apodemus* into three subgenera, with *Sylvaemus* forming a sister clade to *Karstomys*, and these two together sister to the subgenus *Apodemus*. This pattern has been documented in studies using cytochrome *b* (Balasanyan et al., 2018; Darvish et al., 2015; Hoofer et al., 2007) and multigene approaches (Fabre et al., 2012; Suzuki et al., 2008; Michaux et al., 2002), although some studies report alternative topologies (Mezhzherin and Tereshchenko, 2023; Ge et al., 2019; Kryštufek et al., 2012). In our analysis, the split between *Apodemus* and (*Karstomys* + *Sylvaemus*) received moderate support (posterior probability=0.63), which may be explained by incomplete sampling of Asian species that are part of the subgenus *Apodemus* (Steppan and Schenk, 2017; Suzuki et al., 2008, 2003; Zwickl and Hillis, 2002).

While the monophyly of *Karstomys* (represented by *A. mystacinus* and *A. epimelas*) is strongly supported, resolving relationships within *Sylvaemus* proved somewhat challenging. Most nodes within this subgenus received high support (posterior probability>0.9), including the basal position of *A. witherbyi*, the divergence between *A. uralensis* and the clade comprising *A. alpicola* and *A. flavicollis* sensu lato, and the subsequent split between *A. alpicola* and *A.*

flavicollis sensu lato. In contrast, the node separating *A. sylvaticus* from (*A. uralensis* + (*A. alpicola* + *A. flavicollis* sensu lato)) received low support (posterior probability=0.52), indicating uncertainty in its placement. The phylogenetic position of *A. sylvaticus* has consistently been difficult to resolve, even in studies based on the widely used mitochondrial gene cytochrome *b* (Mezhzherin and Tereshchenko, 2023; Olgun Karacan, 2023; Ge et al., 2019; Balasanyan et al., 2018; Yalkovskaya et al., 2018; Herman et al., 2017; Lalis et al., 2016; Darvish et al., 2015; Suzuki et al., 2015; Kryštufek et al., 2012; Chelomina and Atopkin, 2010; Dubey et al., 2009; Suzuki et al., 2008; Balakirev et al., 2007; Hoofer et al., 2007; Michaux et al., 2005, 2004, 2003, 2002; Liu et al., 2004; Reutter et al., 2003; Martin et al., 2000). Depending on the method (e.g., model-based vs. distance-based) and the geographic scope of sampling (e.g., European vs. Asian populations), *A. sylvaticus* has been placed either as sister to *A. flavicollis* sensu lato or in a more basal position within *Sylvaemus*. Similar uncertainties are present in nuclear datasets (Suzuki et al., 2008), although nuclear gene data remain limited in both taxonomic and geographic coverage compared to mitochondrial data.

Multilocus phylogenies of Western Palaearctic *Apodemus* have been conducted on limited sample sets, with most studies analyzing concatenated gene sequences in a supermatrix approach (Ge et al., 2019; Steppan and Schenk, 2017; Fabre et al., 2012; Suzuki et al., 2008, 2003; Michaux et al., 2002). The phylogeny recovered in our study is in full agreement with Fabre et al. (2012) and Michaux et al. (2002), both of which used combined nuclear and mitochondrial loci. However, discrepancies were observed in comparison to other multilocus concatenation-based studies, particularly regarding the placement of *A. sylvaticus* (Suzuki et al., 2003), *A. uralensis* (Suzuki et al., 2008), and the relationship between *A. uralensis* and *A. witherbyi* (Steppan and Schenk, 2017). These discrepancies among studies highlight how

different genes may reflect different evolutionary histories, complicating species delimitation and phylogenetic inference. In this context, the MSC framework, designed to model gene tree discordance relative to the species tree (Douglas et al., 2022; Liu et al., 2009), offers a more robust approach for reconstructing the evolutionary history of *Apodemus*.

Our divergence time estimates were calibrated using the most recent common ancestor (MRCA) of *Apodemus* and *Tokudaia* at ~10.5 Mya, based on the stratigraphic occurrence of *Parapodemus badgleyae* (Kimura et al., 2017), and the *Karstomys/Sylvaemus* split at ~7 Mya (Michaux et al., 2005, 2002). These estimates produced a robust temporal framework consistent with known Miocene fossil records. We estimate the split between *Apodemus* and the *Karstomys* + *Sylvaemus* clade at ~9.76 Mya and the *Karstomys/Sylvaemus* divergence at ~7.4 Mya, both occurring during the Late Miocene. These findings closely align with the estimates of Darvish et al. (2015), reinforcing the role of Late Miocene environmental changes such as aridification and tectonic uplift in the Eastern Mediterranean in shaping early diversification within *Apodemus*.

In the Pliocene, our analysis indicates a series of deeper splits within *Sylvaemus*: *A. witherbyi* diverged around 3.88 Mya, followed by the split between *A. sylvaticus* and *A. uralensis* at 3.48 Mya, and *A. alpicola* diverging from the remaining lineages at 2.7 Mya. These events may reflect expansion into newly available temperate habitats during warmer Pliocene intervals, prior to the onset of severe glaciations.

Further diversification within both *Karstomys* and *Sylvaemus* occurred during the Pleistocene. Within *Sylvaemus*, the divergence between *A. alpicola* and the *A. flavicollis* sensu lato clade is estimated at approximately 1.93 Mya, followed by the split between the Anatolian (TR) and European (SI) lineages of *A. flavicollis* at around 1.36 Mya. Additionally, the divergence between *A. epimelas* and *A. mystacinus* occurred at about 1.57 Mya. These

Pleistocene divergence events likely correspond to glacial–interglacial cycles that generated intermittent barriers to gene flow, promoting allopatric divergence. Compared to previous molecular studies, our estimates for basal splits (e.g., *Karstomys/Sylvaemus*) are congruent, but more recent divergences are consistently younger. For example, Michaux et al. (2005) placed the *A. mystacinus/A. epimelas* split between 4.2–5.1 Mya, while we find it at 1.57 Mya. Similarly, we estimate the divergence of *A. flavicollis* lineages at ~1.36 Mya, compared to 2.2–2.6 Mya in earlier studies (Darvish et al., 2015; Michaux et al., 2004). Our divergence estimate between *A. flavicollis* lineages aligns with Suzuki et al. (2008) who using a Bayesian approach without external calibrations dated the split between *A. flavicollis* (our SI) and *A. ponticus* (our TR) to 0.4–1 Myr, though support varied across molecular markers. These discrepancies may stem from differing calibration strategies: previous studies often used a fixed *Mus*/*Rattus* split at 12 Mya, whereas we employed a murine-internal calibration based on fossil evidence more directly tied to *Apodemus*. Additionally, we used a multispecies coalescent model, which accounts for gene tree discordance and coalescent variance, potentially yielding more precise estimates of speciation timing rather than gene divergence alone.

Collectively, our results emphasize the role of Miocene and Pliocene climatic shifts in shaping major lineages of *Apodemus*, while Pleistocene climatic instability likely drove more recent, finer-scale divergence across Europe and Anatolia.

Morphological divergence

For each morphological structure, significant differences in size and shape among all ten *Apodemus* OTUs are found. *Apodemus mystacinus* and *A. epimelas* are in general the largest. Within the group of *Sylvaemus* mice, *A. flavicollis* from Slovenia is the largest, followed by *A.*

alpicola, while *A. uralensis* from the Czech Republic is the smallest. Janžekovič and Kryštufek (2004) found the same interspecific size pattern in their geometric morphometric study of upper molar size and shape variation in six European *Apodemus* species (*A. agrarius*, *A. epimelas*, *A. flavicollis*, *A. sylvaticus*, *A. uralensis* and *A. alpicola*). When analysing the cranial morphology of six species of the subgenus *Sylvaemus* (*A. alpicola*, *A. flavicollis*, *A. hyrcanicus*, *A. sylvaticus*, *A. uralensis* and *A. witherbyi*), Dúhová (2020) also observed the largest skulls in *A. flavicollis* followed by *A. alpicola*; *A. uralensis* was the smallest in this respect. Differences in skull size can be caused by various environmental conditions, especially the habitat quality and food availability. Larger size can generally be influenced by less stress, e.g. the absence of predators and competitors and the abundance of resources (Abramov et al., 2017). Skull size difference in *Sylvaemus* mice could be linked to habitat, e.g., *A. uralensis* that is primarily associated with open rocky environments (Denys et al., 2017) had the smallest skulls, while *A. flavicollis* mostly living in more productive woodland habitats, the largest. Additionally, variation in body size may be consistent with thermoregulatory expectations. For example, *A. alpicola*, which is endemic to the Alpine region, is larger than other *Sylvaemus* species living in warm environments. On the other hand, intraspecific size variation in *A. mystacinus* was positively associated with the mean minimum January temperature, which is opposite to the predictions of the Bergmann's rule (Yom-Tov and Geffen, 2006).

When looking at the shape variation, all OTU pairs differ significantly from each other, except for the cranial shape variation in the *A. witherbyi* and *A. uralensis* pair from Turkey. According to the average *Rsq* values, *A. mystacinus* shows the greatest differences in mandibular shape variation, *A. epimelas* in cranial shape variation and *A. agrarius* in molar shape variation. The highest classification accuracy of the OTUs is found for *A. alpicola* (97.3% for the mandible

and 100% for the cranium) and *A. agrarius* (100% for the molars). In terms of mandibular shape variation, evident from both CVA and UPGMA, the subgenus *Karstomys* is the most distinct from other congenerics, while in terms of molar shape variation, *A. agrarius* (the only Eurasian representative of the subgenus *Apodemus*) is the most distinctive, followed by *Karstomys*. A good agreement between the phenetic relationships in *Apodemus* with the molecular phylogeny (Bellinvia, 2004; Michaux et al., 2002) and subgeneric taxonomy was found also by Frynta et al. (2006). This statement also seems to apply to other body parts of *Apodemus*. Therefore, Kuncová and Frynta (2009) clearly separated different subgenera in their study on the variability of postcranial and body measurements of seven *Apodemus* species (*A. agrarius*, *A. mystacinus*, *A. hyrcanicus*, *A. witherbyi*, *A. uralensis*, *A. flavicollis* and *A. sylvaticus*). They also reported that multivariate distances based on size-adjusted data showed that the main pattern of morphometric variation was similar to that of the molecular phylogeny. However, morphological differences between species within *Sylvaemus* were small despite substantial differences in habitat preferences (forests, steppe fields, rocks) and differences in locomotion (tendency to dig, jump, climb) (Kuncová and Frynta, 2009). We find that within *Sylvaemus* the most distinct species is *A. alpicola*, characterised by slender mandibles, an elongated rostrum, a constriction in the parietal and zygomatic regions and a compressed braincase. Similar features of the cranial shape of *A. alpicola* have been attributed to the diet of this species, i.e. the absence of hard tree seeds (Reutter et al., 2005) and the higher proportion of insects in the diet (Dúhová, 2020).

Phylogenetic signal in morphometric data

According to mosaic evolution in a phylogenetic context, different morphological structures or trait complexes may have evolved within a group of related organisms under

different scenarios (Cardini and Elton, 2008; Cole et al., 2002). We observe significant phylogenetic structuring in the size and shape variation of each morphological structure analysed, with the exception of cranial shape. Likewise, Jojić et al. (2012) reported that the phenetic relationships among four *Apodemus* species (*A. agrarius*, *A. epimelas*, *A. flavicollis*, and *A. sylvaticus*) inferred from variation in mandibular shape better reflected phylogenetic relationships than those inferred from differences in cranial shape. The lack of a statistically significant phylogenetic signal suggests that related *Apodemus* OTUs are no more similar in cranial shape than phylogenetically unrelated OTUs, so that the evolution of cranial shape is not phylogenetically driven but rather depends on environmental factors. Therefore, the morphological differences in cranial shape may be associated with a high degree of homoplasy, which is determined by ecological constraints through ecophenotypic variation. However, in the absence of modelling of causal factors (e.g., covariation between cranial shape variables and geographic/environmental/ecological variables), this is only an assumption and not a definitive statement. In a complex morphological structure such as the vertebrate cranium, which houses the brain, part of the respiratory system, the masticatory apparatus and various sensory organs, most anatomical components contribute to one or more functions. The anatomical components of the cranium are thus integrated, so that functional adaptations in one component are likely to affect other cranial regions. Therefore, cranial shape represents a mosaic of adaptations and is generally poorly suited as a phylogenetic indicator (Grunstra et al., 2021). Moreover, a lack of concordance between cranial shape variation and phylogeny does not necessarily imply adaptation. It could be genetic drift or simply differences in the pace of evolution.

We discover a significant phylogenetic signal in the variation of mandibular and molar tooth shape. Mandibles and teeth are both involved in food intake and feeding processes, and

such a functional interaction could lead to correlated divergence in response to selection (Michaux et al., 2007). However, the observed pattern of morphological differentiation of mandibles is not identical to that of molars, and only cluster analysis of molar shape confirms the subdivision into three subgenera. This conclusion is consistent with previous results on molar shape variation in six *Apodemus* species obtained in analyses using 2D landmarks on maxillary molars (Janžekovič and Kryštufek, 2004) and geometric morphometrics of the outline of the first upper molar (Helvaci and Çolak, 2021). We also find strong differences in molar shape between *A. agrarius* and all other *Apodemus* OTUs, which is supported by our and other molecular phylogenies (Balasanyan et al., 2018; Steppan and Schenk, 2017; Fabre et al., 2012; Bugarski-Stanojević et al., 2011; Suzuki et al., 2008; Hoofer et al., 2007; Bellinvia, 2004; Michaux et al., 2002). In agreement with the results of Janžekovič and Kryštufek (2004), *A. agrarius* is the most distinct and is characterised by slimmer molars compared to other studied taxa. The highest concordance between the phenogram constructed from molar shape data and our phylogenetic tree suggests that molar shape is the most informative for phylogeny, while the observed interspecific pattern of mandibular shape may be due to ecological factors interfering with the pattern of genetic divergence. That mandibles and molars can provide a contradictory picture of the evolution of *Apodemus* mice was shown by Ledevin et al. (2012), who demonstrated that the mandibular shape of five Chinese *Apodemus* species (*A. peninsulae*, *A. uralensis*, *A. agrarius*, *A. draco*, and *A. latronum*) appears to vary in response to local conditions, blurring any phylogenetic or ecological pattern, while the evolution of molar shape appears to be primarily determined by the degree of genetic differentiation.

As Caumul and Polly (2005) noted, the skull, mandible and teeth differ in their responses to environmental selection pressures not only because of their different functions and the

different number of underlying genes that control their shape, but an important difference between them is the different pattern of ontogenetic development. While the cranium and mandible tend to undergo bone remodeling and respond plastically through growth even after the animal is weaned (Renaud and Auffray, 2010; Renaud et al., 2010), molars, once erupted, are only subject to wear, a process that only slightly affects the crown outline (Renaud, 2005). For this reason, they are less sensitive to direct environmental influences (Ledevin et al., 2012), exhibit less ecophenotypic variation (Rychlik et al., 2006; Renaud, 2005) and evolve more slowly than the cranium and mandible. Based on a significant correlation between molar tooth shape and cytochrome *b* gene sequence divergence in shrews and marmots, Polly (2003, 2001) suggested that tooth morphology could serve as a proxy for phylogenetic divergence. A strong correlation between genetic and morphological distances was found in molars of the murine genus *Mus* (Ledevin et al., 2016; Macholán, 2006). Our study shows that molar shape contains a considerable amount of phylogenetic information sufficient to clarify relationships at the subgeneric level, but not at the species level. Morphometric data in general, no matter how strong the phylogenetic signal they contain, are not suitable markers for the phylogenetic reconstruction of a clade (Varón-González et al., 2020; Klingenberg and Gidaszewski, 2010). This result is important not only from the taxonomic perspective of extant rodent species, but also for reconstructing the evolutionary history of extinct species, most of which are known from isolated molars.

CONCLUSION

In this study, we focused on the Western Palearctic species of the genus *Apodemus* and adopted an integrated approach combining molecular phylogenetics with geometric morphometrics. To investigate the contribution of phylogenetic signal and adaptive processes to morphological variability in these rodents, we used mitochondrial and nuclear markers from GenBank (cytochrome *b*, *12S rRNA*, D-loop, *COI*, *IRBP*, *RAG1*, *I7*, *vWF*) and applied a two-dimensional geometric morphometric analysis to the mandible, cranium and upper molars, three anatomical structures traditionally used in studies of small mammal morphology. A phylogenetic signal is evident in the size and shape variation of each morphological structure analysed, with the exception of cranial shape, supporting a mosaic model of morphological evolution within *Apodemus*. While morphometric data are less suitable than molecular data for reconstructing phylogenies, molars stand out as a more reliable indicator of phylogenetic divergence than the mandible or cranium. This is because molars are less influenced by environmental factors, exhibit less ecophenotypic variation, and evolve more slowly. Consequently, molar shape effectively distinguishes *Apodemus* subgenera and may have broader applications in other rodents. This is particularly important for fossil taxa, where molar remains are often the only material available and molecular data are unattainable, underscoring the value of molar morphology for reconstructing evolutionary histories of extinct species and informing taxonomy of extant rodents.

REFERENCES

Abramov, S.A., Lopatina, N.V., Litvinov, Y.N., 2017. Cranial size and shape variation in isolated populations of the Olkhon mountain vole (*Alticola olchonensis* Litvinov, 1960). Zoology 123: 91-100.

Balakirev, A.E., Baskevich, M.I, Gmyl, A.P., Okulova, N.M., Andreeva, T.A., Sokolenko, O.V., Malygin, V.M., Khlyap, L.A., Oparin, M.L., Orlov, V.N., 2007. On the taxonomic rank of ciscaucasicus and its relationships with the pygmy wood mouse *Sylvaemus uralensis* inferred from the mtDNA cytochrome *b* gene sequence. Russ. J. Genet. 43: 1386-1399.

Balasanyan, V., Yavruyan, E., Somerová, B., Abramjan, A., Landová, E., Munclinger, P., Frynta, D., 2018. High Diversity of mtDNA Haplotypes Confirms Syntopic Occurrence of Two Field Mouse Species *Apodemus uralensis* and *A. witherbyi* (Muridae: Apodemus) in Armenia. Russ. J. Genet. 54: 687-697.

Barčiová, L., Macholán, M., 2009. Morphometric key for the discrimination of two wood micespecies, *Apodemus sylvaticus* and *A. flavicollis*. Acta Zool. Acad. Sci. Hung. 55: 31-38.

Bellinvia, E., 2004. A phylogenetic study of the genus *Apodemus* by sequencing the mitochondrial DNA control region. J. Zool. Syst. Evol. Res. 42: 289-297.

Bookstein, F.L., 1991. Morphometric Tools for Landmark Data. Cambridge University Press, Cambridge, UK.

Bouckaert, R.R., Drummond, A.J., 2017. bModelTest: Bayesian phylogenetic site model averaging and model comparison. BMC Evol. Biol. 17: 42.

Bouckaert, R., Vaughan, T.G., Barido-Sottani, J., Duchêne, S., Fourment, M., Gavryushkina, A., Heled, J., Jones, G., Kühnert, D., De Maio, N., Matschiner, M., Mendes, F.K., Müller, N.F., Ogilvie, H.A., du Plessis, L., Popinga, A., Rambaut, A., Rasmussen, D., Siveroni, I., Suchard, M.A., Wu, C-H., Xie, D., Zhang, C., Stadler, T., Drummond, A.J., 2019. BEAST 2.5: An advanced software platform for Bayesian evolutionary analysis. PLoS Comp. Biol. 15: e1006650.

Bugarski-Stanojević, V., Blagojević, J., Stamenković, G., Adnađević, T., Giagia-Athanasopoulou, E., Vujošević, M., 2011. Comparative study of the phylogenetic structure in six *Apodemus* species (Mammalia, Rodentia) inferred from ISSR-PCR data. Syst. Biodivers. 9: 95-106.

Burgin, C.J., Wilson, D.E., Mittermeier, R.A., Rylands, A.B., Lacher, T.E., Sechrest, W., 2020. Illustrated Checklist of the Mammals of the World. Volume 1. Monotremata to Rodentia. Lynx Editions, Barcelona, Spain.

Cardini, A., Elton, S., 2008. Does the skull carry a phylogenetic signal? Evolution and modularityin the guenons. Biol. J. Linn. Soc. 93: 813-834.

Caumul, R., Polly, P.D., 2005. Phylogenetic and environmental components of morphological variation: skull, mandible, and molar shape in marmots (*Marmota*, Rodentia). Evolution 59: 2460-2472.

Chelomina, G.N., Atopkin, D.M., 2010. Molecular genetic evidence of a deep phylogenetic discontinuity between the asian and european races of pygmy wood mouse based on the mitochondrial cytochrome *b* gene variation. Mol. Biol. 44: 699-708.

Çolak, R., Çolak, E., Yiğit, N., Kandemir, I., Sözen, M., 2007. Morphometric and biochemical variation and the distribution of the genus *Apodemus* (Mammalia: Rodentia) in Turkey. Acta Zool. Acad. Sci. Hung. 53: 239-256.

Cole, T.M., Lele, S., Richtsmeier, J.T., 2002. A parametric bootstrap approach to the detection of phylogenetic signals in landmark data. In: Macleod, N., Forey, P (Eds.) Morphology, shape and phylogeny. Taylor and Francis, London, UK. 194-219.

Darvish, J., Mohammadi, Z., Ghorbani, F., Mahmoudi, A., Dubey, S., 2015. Phylogenetic Relationships of *Apodemus* Kaup, 1829 (Rodentia: Muridae) Species in the Eastern

Mediterranean Inferred from Mitochondrial DNA, with Emphasis on Iranian Species. J. Mamm. Evol. 22: 583-595.

Darvish, J., Mohammadi, Z., Ghorbani, F., Mostafavi, E., 2014. Morphological Morphometric Characterisation of the Eastern Broad-toothed Field Mouse *Apodemus mystacinus* (Rodentia: Muridae) from Zagros Mountains, north-western Iran. Acta Zool. Bulg. 66: 461-468.

Denys, C., Taylor, P. J., Aplin, P., 2017. Family Muridae (true mice and rats, gerbils and relatives). In: Wilson, D.E., Lacher, T.E., Mittermeier, R.A (Eds.) Handbook of the mammals of the world, Volume 7: Rodents II. Lynx Editions, Barcelona, Spain. 536-886.

Douglas, J., Jiménez-Silva, C.L., Bouckaert, R., 2022. StarBeast3: Adaptive Parallelized Bayesian Inference under the Multispecies Coalescent. Syst. Biol. 71: 901-916.

Dryden, I.L., Mardia, K.V., 1998. Statistical Shape Analysis. John Wiley and Sons, New York, USA.

Dubey, S., Michaux, J., Brünner, H., Hutterer, R., Vogel, P., 2009. False phylogenies on wood mice due to cryptic cytochrome-*b* pseudogene. Mol. Phylogen. Evol. 50: 633-641.

Dúhová, K., 2020. Phylogeny and cranial geometric morphometry of selected *Apodemus* species (Rodentia: Murinae). M.Sc. thesis, Faculty of Science, Masaryk University, Brno, Czech Republic.

Edgar, R.C., 2004. MUSCLE: multiple sequence alignment with high accuracy and high throughput. Nucleic Acids Res. 32: 1792-1797.

Edgington, E.S., 1995. Randomization Tests. Marcel Dekker, New York, USA.

Fabre, P-H., Hautier, L., Dimitrov, D., Douzery, E.J.P., 2012. A glimpse on the pattern of rodent diversification: a phylogenetic approach. Evol. Biol. 12: 88.

Felsenstein, J.,2002. Quantitative characters, phylogenies, and morphometrics. In: MacLeod, N., Forey, P (Eds.) Morphology, shape, and phylogeny. Taylor and Francis, London, UK. 27-44.

Filippucci, M.G., Storch, G., Macholán, M., 1996. Taxonomy of the genus *Sylvaemus* in western Anatolia—morphological and electrophoretic evidence (Mammalia: Rodentia: Muridae). Senckenb. Biol.7 5: 1-14.

Frynta, D., Mikulová, P., Vohralík, V., 2006. Skull shape in the genus *Apodemus*: phylogenetic conservatism and/or adaptation to local conditions. Acta Theriol. 51: 139-153.

Ge, D., Feijó, A., Cheng, J., Lu, L., Liu, R., Abramov, A. V., Xia, L., Wen, Z., Zhang, W., Shi, L., Yang, Q., 2019. Evolutionary history of field mice (Murinae: *Apodemus*), with emphasis on morphological variation among species in China and description of a new species. Zool. J. Linn. Soc. 187: 518-534.

Good, P., 1994. Permutation Test: A Practical Guide to Resampling Methods for Testing Hypotheses. Springer-Verlag, New York, USA.

Grunstra, N.D.S., Bartsch, S.J., Le Maître, A., Mitteroecker, P., 2021. Detecting phylogenetic signal and adaptation in papionin cranial shape by decomposing variation at different spatial scales. Syst. Biol. 70: 694-706.

Helvaci, Z., Çolak, E., 2021. New Data on the Taxonomy of the Genus *Apodemus* Kaup, 1829 (Mammalia: Rodentia) in Turkey: a Geometric Morphometric Approach. Acta Zool. Bulg. 73: 503-509.

Herman, J.S., Jóhannesdóttir, F., Jones, E.P., McDevitt, A.D., Michaux, J.R., White, T.A., Wójcik, J.M., Searle, J.B., 2017. Post-glacial colonization of Europe by the wood mouse,

Apodemus sylvaticus: evidence of a northern refugium and dispersal with humans. Biol. J. Linn. Soc. 120: 313-332.

Hille, A., Tarkhnishvili, D., Meinig, H., Hutterer, R., 2002. Morphometric, biochemical and molecular traits in Caucasian wood mice (*Apodemus/Sylvaemus*), with remarks on species divergence. Acta Theriol. 47: 389-416.

Hoang, D.T., Chernomor, O., von Haeseler, A., Minh, B.Q., Vinh L.S., 2018. UFBoot2: Improving the ultrafast bootstrap approximation. Mol. Biol. Evol. 35: 518-522.

Hoofer, S.R., Gaschak, S., Dunina-Barkovskaya, Y., Makluk, J., Meeks, H.N., Wickliffe, J.K., Baker, R.J., 2007. New information for systematics, taxonomy, and phylogeography of the rodent genus *Apodemus* (*Sylvaemus*) in Ukraine. J. Mammal. 88: 330-342.

IBM Corp., 2017. IBM SPSS Statistics for Windows, Version 25. Armonk, NY: IBM Corp.

Janžekovič, F., Kryštufek, B., 2004. Geometric morphometry of the upper molars in European wood mice *Apodemus*. Folia Zool. 53: 47-55.

Jojić, V., Bugarski-Stanojević, V., Blagojević, J., Vujošević, M., 2014. Discrimination of the sibling species *Apodemus flavicollis* and *A. sylvaticus* (Rodentia, Muridae). Zool. Anz. 253: 261-269.Jojić, V., Nenadović, J., Blagojević, J., Paunović, M., Cvetković, D., Vujošević, M., 2012. Phenetic relationships among four *Apodemus* species (Rodentia, Muridae) inferred from skull variation. Zool. Anz. 251: 26-37.

Kerr, E., Cornette, R., Gomes Rodrigues, H., Renaud, S., Chevret, P., Tresset, A., Herrel, A., 2017. Can functional traits help explain the coexistence of two species of *Apodemus*? Biol. J. Linn. Soc. 122: 883-896.

Kimura, Y., Flynn, L.J., Jacobs, L.L., 2017. Early late miocene murine rodents from the upper part of the Nagri formation, Siwalik group, Pakistan, with a new fossil calibration point for the Tribe Apodemurini (*Apodemus/Tokudaia*). Foss. Impr. 73: 197-212.

Klingenberg, C.P., 2011. MorphoJ: an integrated software package for geometric morphometrics. Mol. Ecol. Resour. 11: 353-357.

Klingenberg, C.P., 2013. Visualizations in geometric morphometrics: how to read and how to make graphs showing shape changes. Hystrix 24: 15.

Klingenberg, C.P., Gidaszewski, N.A., 2010. Testing and quantifying phylogenetic signals and homoplasy in morphometric data. Syst. Biol. 59: 245-261.

Knitlova, M., Horaček, I., 2017. Late Pleistocene-Holocene paleobiogeography of the genus *Apodemus* in Central Europe. PLoS One 12: e0173668.

Kryštufek, B., Janžekovič, F., Hutterer, R., Klenovšek, T., 2016. Morphological evolution of the skull in closely related bandicoot rats: a comparative study using geometric morphometrics. Hystrix 27: 163-169.

Kryštufek, B., Lužnik, M., Buzan, E.V., 2012. Mitochondrial cytochrome *b* sequences resolve the taxonomy of field mice (*Apodemus*) in the western Balkan refugium. Acta Theriol. 57: 1-7.

Kryštufek, B., Vohralík, V., 2009. Mammals of Turkey and Cyprus. Rodentia II: Cricetinae, Muridae, Spalacidae, Calomyscidae, Capromyidae, Hystricidae, Castoridae. Založba Annales, Koper, Slovenia.

Kryštufek, B., Stojanovski, L., 1996. *Apodemus sylvaticus stankovici* is a synonym of *Apodemus flavicollis*. Folia Zool. 45: 1-7.

Kuncová, P., Frynta, D., 2009. Interspecific morphometric variation in the postcranial skeleton in the genus *Apodemus*. Belg. J. Zool. 139: 133-146.

Lachenbruch, P.A., 1967. An almost unbiased method of obtaining confidence intervals for the probability of misclassification in discriminant analysis. Biometrics 23: 639-645.

Lalis, A., Leblois, R., Liefried, S., Ouarour, A., Beeravolu, C.R., Michaux, J., Hamani, A., Denys, C., Nicolas, V., 2016. New molecular data favour an anthropogenic introduction of the wood mouse (*Apodemus sylvaticus*) in North Africa. J. Zool. Syst. Evol. Res. 54: 1-12.

Latinne, A., Navascués, M., Pavlenko, M., Kartavtseva, I., Ulrich, R.G., Tiouchichine, M-L., Catteau, G., Sakka, H., Quéré, J-P., Chelomina, G., Bogdanov, A., Stanko, M., Hang, L., Neumann, K., Henttonen, H., Michaux, J., 2020. Phylogeography of the striped field mouse, *Apodemus agrarius* (Rodentia: Muridae), throughout its distribution range in the Palaearctic region. Mamm. Biol. 100: 19-31.

Larsson, A., 2014. AliView: a fast and lightweight alignment viewer and editor for large data sets. Bioinformatics 30: 3276-3278.

Ledevin, R., Chevret, P., Ganem, G., Britton-Davidian, J., Hardouin, E.A., Chapuis, J-L., Pisanu, B., Mathias, M.D.L., Schlager, S., Auffray, J-C., Renaud, S., 2016. Phylogeny and adaptation shape the teeth of insular mice. Proc. R. Soc. B283: 20152820.

Ledevin, R., Quéré, J-P., Michaux, J.R., Renaud, S., 2012. Can tooth differentiation help to understand species coexistence? The case of wood mice in China. J. Zool. Syst. Evol. Res. 50: 315-327.

Liu, Q., Chen, P., He, K., Kilpatrick, C. W., Liu, S-Y., Yu, F-H., Jiang, X-L., 2012. Phylogeographic study of *Apodemus ilex* (Rodentia: Muridae) in southwest China. PLoS One 7: e31453.

Liu, X., Wei, F., Li, M., Jiang, X., Feng, Z., Hu, J., 2004. Molecular phylogeny and taxonomy of wood mice (genus *Apodemus* Kaup, 1829) based on complete mtDNA cytochrome *b* sequences, with emphasis on Chinese species. Mol. Phylogen. Evol. 33: 1-15.

Liu, L., Yu, L., Kubatko, L., Pearl, D.K., Edwards, S.V., 2009. Coalescent methods for estimating phylogenetic trees. Mol. Phylogen. Evol. 53: 320-328.

Lu, X., Ge, D., Xia, L., Huang, C., Yang, Q., 2014. Geometric morphometric study of the skull shape diversification in Sciuridae (Mammalia, Rodentia). Integr. Zool. 9: 231-245.

Macholán, M., 2006. A geometric morphometric analysis of the shape of the first upper molar in mice of the genus *Mus* (Muridae, Rodentia). J. Zool. 270: 672-681.

Martin, Y., Gerlach, G., Schlötterer, C., Meyer, A., 2000. Molecular phylogeny of european muroid rodents based on complete cytochrome *b* sequences. Mol. Phylogen. Evol. 16: 37-47.

Martín-Suárez, E., Mein, R., 1998. Revision of the genera *Parapodemus*, *Apodemus*, *Rhagarnys* and *Rhagapodemus* (Rodentia, Mammalia). GEOBIOS 31: 87-97.

Mezhzherin, S.V., Tereshchenko, V.O., 2023. Taxonomic Hierarchy and Evolutionary Scenario of the Genus Group *Apodemus* s. l. (Muridae) of the Palaearctic based on Genetic Differentiation in the cyt-b Gene. Zoodiversity 57: 1-12.

Michaux, J.R., Bellinvia, E., Lymberakis, P., 2005. Taxonomy, evolutionary history and biogeography of the broad-toothed field mouse (*Apodemus mystacinus*) in the eastern

Mediterranean area based on mitochondrial and nuclear genes. Biol. J. Linn. Soc. 85: 53-63.

Michaux, J.R., Chevret, P., Filippucci, M-G., Macholan, M., 2002. Phylogeny of the genus *Apodemus* with a special emphasis on the subgenus *Sylvaemus* using the nuclear IRBP gene and two mitochondrial markers: cytochrome *b* and 12S rRNA. Mol. Phylogen. Evol. 23: 123-136.

Michaux, J., Chevret, P., Renaud, S., 2007. Morphological diversity of Old World rats and mice (Rodentia, Muridae) mandible in relation with phylogeny and adaptation. J. Zool. Syst. Evol. Res. 45: 263-279.

Michaux, J., Kinet, S., Filippucci, M.-G., Libois, R., Besnard, A., Catzeflis, F., 2001. Molecular identification of three sympatric species of wood mice (*Apodemus sylvaticus*, *A. flavicollis*, *A. alpicola*) in western Europe (Muridae: Rodentia). Mol. Ecol. Notes 1: 260-263.

Michaux, J.R., Libois, R., Paradis, E., Filippucci, M-G., 2004. Phylogeographic history of the yellow-necked field mouse (*Apodemus flavicollis*) in Europe and in the Near and Middle East. Mol. Phylogen. Evol. 32: 788-798.

Michaux, J.R., Magnanou, E., Paradis, E., Nieberding, C., Libois, R., 2003. Mitochondrial phylogeography of the Wood mouse (*Apodemus sylvaticus*) in the Western Palearctic region. Mol. Ecol. 12: 685-697.

Musser, G.G., Brothers, E.M., Carleton, M.D., Hutterer, R., 1996. Taxonomy and distributional records of Oriental and European *Apodemus*, with a review of the *Apodemus-Sylvaemus* problem. BzB46: 143-190.

Musser, G.G., Carleton, M.D., 2005. Superfamily Muroidea. In: Wilson, D.E., Reeder, D.M (Eds.) Mammal species of the world: a taxonomic and geographic reference. Johns Hopkins University Press, Baltimore, USA. 894-1531.

Niethammer, J., 1969. Zur frage der introgression bei den waldmäusen *Apodemus sylvaticus* und *A. flavicollis* (Mammalia, Rodentia). Zeitschrift Zoologische Systematik Evolutionsforschung 7: 77-127.

Okulova, N.M., Bogdanov, A.S., Baskevich, M.I., Orlov, V.N., Antonets, N.V., Popova, Yu.V., Lavrenchenko, L.A., 2019. Skull Sizes and Proportions in Western Palearctic Wood Mice (*Sylvaemus*, Muridae, Rodentia) from Eastern Europe: 1. Interspecific Variability. Biol. Bull. 46: 973-987.

Olgun Karacan, G., 2023. Uncovering hidden diversity: new phylogeographic pattern of *Apodemus mystacinus* (Danford and Alston, 1877) in Turkey and Iran. Russ. J. Genet. 59: 53-60.

Polly, P.D., 2001. On morphological clocks and paleophylogeography: towards a timescale for *Sorex* hybrid zones. Genetica 112: 339-357.

Polly, P.D., 2003. Paleophylogeography: the tempo of geographic differentiation in marmots (*Marmota*). J. Mammal. 84: 369-384.

Rambaut, A., Drummond, A.J., Xie, D., Baele, G., Suchard, M.A., 2018. Posterior summarization in Bayesian phylogenetics using Tracer 1.7. Syst. Biol. 67: 901-904.

Renaud, S., 2005. First upper molar and mandible shape of wood mice (*Apodemus sylvaticus*) from northern Germany: ageing, habitat and insularity. Mamm. Biol. 70: 157-170.

Renaud, S., Auffray, J-C., 2010. Adaptation and plasticity in insular evolution of the house mouse mandible. J. Zool. Syst. Evol. Res. 48: 138-150.

Renaud, S., Auffray, J-C., de La Porte, S., 2010. Epigenetic effects on the mouse mandible: common features and discrepancies in remodeling due to muscular dystrophy and response to food consistency. BMC Evol. Biol. 20: 18.

Renaud, S., Chevret, P., Michaux, J., 2007. Morphological vs. molecular evolution: Ecology and phylogeny, both shape the mandible of rodents. Zool. Scr. 36: 525-535.

Renaud, S., Michaux, J.R., 2003. Adaptive latitudinal trends in the mandible shape of *Apodemus* wood mice. J. Biogeogr. 30: 1617-1628.

Reutter, B.A., Bertouille, E., Vogel, P., 2005. The diet of the Alpine mouse *Apodemus alpicola* in the Swiss Alps. Mamm. Biol. 70: 147-155.

Reutter, B.A., Petit, E., Brünner, H., Vogel, P., 2003. Cytochrome *b* haplotype divergences in West European *Apodemus*. Mamm. Biol. 68: 153-164.

Revell, L.J., 2024. phytools 2.0: an updated R ecosystem for phylogenetic comparative methods (and other things). PeerJ 12: e16505.

Rohlf, F.J., 1999. Shape statistics: Procrustes superimpositions and tangent spaces. J. Classif. 16: 197-223.

Rohlf, F.J., 2015a. TpsDig. Version 2.30. Department of Ecology and Evolution, State University of New York, Stony Brook NY, USA.

Rohlf, F.J., 2015b. The tps series of software. Hystrix 26: 9-12.

Rohlf, F.J., Marcus, L.F., 1993. A revolution in morphometrics. TREE 8: 129-132.

Rohlf, F.J., Slice, D., 1990. Extensions of the Procrustes method for the optimal superimposition of landmarks. Syst. Zool. 39: 40-59.

Rychlik, L., Ramalhinho, G., Polly, P.D., 2006. Response to environmental factors and competition: skull, mandible and tooth shapes in Polish water shrews (*Neomys*, Soricidae, Mammalia). J. Zool. Syst. Evol. Res. 44: 339-351.

Schenk, J.J., Rowe, K.C., Steppan, S.J., 2013. Ecological opportunity and incumbency in the diversification of repeated continental colonizations by muroid rodents. Syst. Biol. 62: 837-864.

Steppan, S.J., Schenk, J.J., 2017. Muroid rodent phylogenetics: 900-species tree reveals increasing diversification rates. PLoS One 12: e0183070.

Suzuki, H., Filippucci, M.G., Chelomina, G.N., Sato, J.J., Serizawa, K., Nevo, A., 2008. A Biogeographic View of *Apodemus* in Asia and Europe Inferred From Nuclear and Mitochondrial Gene Sequences. Biochem. Genet. 46: 329-346.

Suzuki, H., Sato, J.J., Tsuchiya, K., Luo, J., Zhang, Y-P., Wang, Y-X., Jiang, X-L., 2003. Molecular phylogeny of wood mice (*Apodemus*, Muridae) in East Asia. Biol. J. Linn. Soc. 80: 469-481.

Suzuki, Y., Tomozawa, M., Koizumi, Y., Tsuchiya, K., Suzuki, H., 2015. Estimating the molecular evolutionary rates of mitochondrial genes referring to Quaternary ice age events with inferred population expansions and dispersals in Japanese *Apodemus*. BMC Evol. Biol. 15: 187.

Tvrtković, N., 1979. Unterscheidung und determination der «zwillingsarten» aus subgenus *Sylvemus* Ognev et Vorobiev, 1923 (Rodentia, Mammalia). RAD Jugoslovenske akademije znanosti i umjetnosti, Razred za prirodne znanosti 383: 155-186 (in Croatian with German summary).

Varón-González, C., Whelan, S., Klingenberg, C.P., 2020. Estimating phylogenies from shape and similar multidimensional data: why it is not reliable. Syst. Biol. 69: 863-883.

Vaughan, T.G., 2017. IcyTree: Rapid browser-based visualization for phylogenetic trees and networks. Bioinformatics 33: 2392-2394.

Wong, T.K.F., Ly-Trong, N., Ren, H., Banos, H., Roger, A.J., Susko, E., Bielow, C., De Maio, N., Goldman, N., Hahn, M.W., Huttley, G., Lanfear, R., Minh B.Q., 2025. IQ-TREE 3: Phylogenomic Inference Software using Complex Evolutionary Models. Submitted. https://ecoevorxiv.org/repository/view/8916/

Yalkovskaya, L., Sibiryakov, P., Borodin, A., 2022. Phylogeography of the striped field mouse (*Apodemus agrarius* Pallas, 1771) in light of new data from central part of Northern Eurasia. PLoS One 17: e0276466.

Yalkovskaya, L.E., Sibiryakov, P.A., Zykov, S.V., 2018. Genetic variability in the yellow-necked field mouse (*Sylvaemus flavicollis* Melch., 1834, Muridae, Rodentia) at the eastern border of the range. Russ. J. Genet. 54: 643-651.

Yom-Tov, Y., Geffen, E., 2006. Geographic variation in body size: the effects of ambient temperature and precipitation. Oecologia 148: 213-218.

Zwickl, D.J., Hillis, D.M., 2002. Increased Taxon Sampling Greatly Reduces Phylogenetic Error (K Crandall, Ed.). Syst. Biol. 51: 588-598.

HYSTRIX
the Italian Journal of Mammalogy

Table 1. Localities and sample sizes (N) of *Apodemus* spp. male (M), female (F) and unknown sex (U) specimens (mandibles, crania, and upper molars) analysed in this study.

Species	Locality	OTU	Mandible N (M, F, U)	Cranium N (M, F, U)	Molars N (M, F, U)
A. agrarius	Primorska (Slovenia)	*A. agrarius*	27 (2, 3, 22)	26 (2, 3, 21)	26 (2, 3, 21)
A. alpicola	Silbertal, Pfunds (Austria)	*A. alpicola*	37 (12, 15, 10)	31 (12, 15, 4)	34 (11, 13, 10)
A. flavicollis	Kočevski Rog (Slovenia)	*A. flavicollis* SI	29 (0, 0, 29)	30 (0, 0, 30)	31 (0, 0, 31)
	Anatolia (Turkey)	*A. flavicollis* TR	20 (11, 6, 3)	20 (13, 6, 1)	22 (13, 6, 3)
A. sylvaticus	Sečoveljske soline, Kranjska gora (Slovenia)	*A. sylvaticus*	24 (1, 4, 19)	26 (1, 4, 21)	25 (1, 4, 20)
A. uralensis	Hodonin (Czech Republic)	*A. uralensis* CZ	18 (10, 4, 4)	24 (12, 8, 4)	25 (12, 8, 5)
	Anatolia (Turkey)	*A. uralensis* TR	25 (12, 10, 3)	29 (15, 10, 4)	32 (15, 9, 8)
A. witherbyi	Anatolia (Turkey)	*A. witherbyi*	26 (17, 7, 2)	27 (20, 7, 0)	29 (20, 7, 2)
A. epimelas	Pelješac (Croatia), Dodoši (Montenegro)	*A. epimelas*	28 (5, 3, 20)	33 (9, 4, 20)	35 (9, 4, 22)
A. mystacinus	Anatolia (Turkey)	*A. mystacinus*	30 (16, 11, 3)	29 (16, 10, 3)	27 (16, 9, 2)
Total			264	275	286

Table 2. Classification accuracy (in %) obtained by Discriminant Function Analysis, assessed using leave-one-out cross-validation, of OTUs for the mandible.

	{1}	{2}	{3}	{4}	{5}	{6}	{7}	{8}	{9}	{10}	Total
A. agrarius {1}	**92.6**	0.0	0.0	3.7	0.0	0.0	0.0	0.0	3.7	0.0	100.0
A. alpicola {2}	2.7	**97.3**	0.0	0.0	0.0	0.0	0.0	0.0	0.0	0.0	100.0
A. sylvaticus {3}	0.0	0.0	**66.7**	4.2	0.0	0.0	12.5	12.5	0.0	4.2	100.0
A. witherbyi {4}	0.0	0.0	7.7	**61.5**	3.8	0.0	7.7	3.8	3.8	11.5	100.0
A. epimelas {5}	0.0	0.0	0.0	3.6	**96.4**	0.0	0.0	0.0	0.0	0.0	100.0
A. mystacinus {6}	0.0	0.0	0.0	0.0	3.3	**96.7**	0.0	0.0	0.0	0.0	100.0
A. flavicollis SI {7}	0.0	0.0	10.3	10.3	3.4	0.0	**69.0**	3.4	0.0	3.4	100.0
A. flavicollis TR {8}	0.0	0.0	0.0	20.0	0.0	0.0	20.0	**60.0**	0.0	0.0	100.0
A. uralensis CZ {9}	11.1	0.0	0.0	0.0	0.0	0.0	0.0	0.0	**83.3**	5.6	100.0
A. uralensis TR {10}	0.0	0.0	4.0	8.0	0.0	0.0	4.0	4.0	4.0	**76.0**	100.0

Table 3. Classification accuracy (in %) obtained by Discriminant Function Analysis, assessed using leave-one-out cross-validation, of OTUs for cranium.

	{1}	{2}	{3}	{4}	{5}	{6}	{7}	{8}	{9}	{10}	Total
A. agrarius {1}	**96.2**	0.0	0.0	0.0	0.0	0.0	3.8	0.0	0.0	0.0	100.0
A. alpicola {2}	0.0	**100.0**	0.0	0.0	0.0	0.0	0.0	0.0	0.0	0.0	100.0
A. sylvaticus {3}	0.0	0.0	**92.3**	0.0	0.0	0.0	0.0	0.0	3.8	3.8	100.0
A. witherbyi {4}	0.0	0.0	0.0	**63.0**	0.0	0.0	0.0	0.0	0.0	37.0	100.0
A. epimelas {5}	0.0	0.0	0.0	0.0	**100.0**	0.0	0.0	0.0	0.0	0.0	100.0
A. mystacinus {6}	0.0	0.0	0.0	0.0	0.0	**96.6**	0.0	3.4	0.0	0.0	100.0
A. flavicollis SI {7}	0.0	0.0	3.3	0.0	0.0	0.0	**76.7**	10.0	10.0	0.0	100.0
A. flavicollis TR {8}	5.0	0.0	0.0	10.0	0.0	0.0	5.0	**60.0**	5.0	15.0	100.0
A. uralensis CZ {9}	4.2	0.0	0.0	8.3	0.0	0.0	12.5	8.3	**54.2**	12.5	100.0
A. uralensis TR {10}	0.0	0.0	0.0	10.3	0.0	0.0	6.9	13.8	13.8	**55.2**	100.0

960 **Table 4.** Classification accuracy (in %) obtained by Discriminant Function Analysis, assessed
961 using leave-one-out cross-validation, of OTUs for upper molars.

	{1}	{2}	{3}	{4}	{5}	{6}	{7}	{8}	{9}	{10}	Total
A. agrarius {1}	**100.0**	0.0	0.0	0.0	0.0	0.0	3.8	0.0	0.0	0.0	100.0
A. alpicola {2}	0.0	**70.6**	0.0	5.9	0.0	0.0	0.0	2.9	2.9	17.6	100.0
A. sylvaticus {3}	0.0	0.0	**44.0**	20.0	0.0	0.0	8.0	16.0	12.0	0.0	100.0
A. witherbyi {4}	0.0	10.3	6.9	**62.1**	6.9	0.0	0.0	6.9	0.0	6.9	100.0
A. epimelas {5}	0.0	0.0	0.0	2.9	**91.4**	2.9	2.9	0.0	0.0	0.0	100.0
A. mystacinus {6}	0.0	0.0	0.0	3.7	11.1	**63.0**	18.5	0.0	0.0	3.7	100.0
A. flavicollis SI {7}	0.0	3.2	9.7	3.2	3.2	6.5	**64.5**	9.7	0.0	0.0	100.0
A. flavicollis TR {8}	0.0	4.5	9.1	4.5	0.0	4.5	22.7	**40.9**	0.0	13.6	100.0
A. uralensis CZ {9}	0.0	4.0	8.0	0.0	0.0	0.0	4.0	0.0	**80.0**	4.0	100.0
A. uralensis TR {10}	0.0	6.3	6.3	0.0	0.0	3.1	6.3	0.0	3.1	**75.0**	100.0

962
963

Table 5. Phylogenetic signal in morphometric data. Tree lengths are calculated by weighted squared-change parsimony and *P* values are from permutation tests against the null hypothesis of no phylogenetic signal.

	Size (centroid size)		Shape (Procrustes coordinates)	
	Tree length	*P* value	Tree length	*P* value
mandible	7.8898	0.0243	0.0055	0.0215
cranium	34.6699	0.0205	0.0021	0.3135
upper molars	0.8895	0.0177	0.0047	0.0023

Figure 1. Landmarks collected on images of the mandible in labial view (A), cranium in ventral view (B), and upper molars in occlusal view (C).

Figure 2. The maximum clade credibility phylogenetic relationship of a tribus Apodemini from the Western Palearctic inferred by Bayesian multispecies multilocus coalescent analyses in BEAST 2. Apodemini MRCA calibration point of about 10.7 Myr was used after Kimura et al. (2017). Node bars indicate the 95% credible interval of the posterior density of divergence times which is expressed in millions of years (Myr) ago since presence. The posterior median of divergence times are in bold, depicted on the left-hand side of each node, while posterior support for node splits are on the right-hand side of each node. *Apodemus* subgenera are colored as: *Sylvaemus* (green), *Karstomys* (blue) and *Apodemus* (red).

Figure 3. CVA scatterplots of the first and second CV axes for the mandible. Shape changes along CV axes are visualized by warped outline drawings that are magnified two times.

Figure 4. CVA scatterplots of the first and second CV axes for the cranium. Shape changes along CV axes are visualized by warped outline drawings that are magnified two times.

Figure 5. CVA scatterplots of the first and second CV axes for upper molars. Shape changes along CV axes are visualized by warped outline drawings that are magnified two times.

Figure 6. Co-phylogenetic comparison between the MSC phylogeny (left) and the UPGMA phenogram based on Procrustes distances among mean OTU mandibular shapes (right). Horizontal red lines connect corresponding taxa across the two trees. Mean mandibular shapes for each *Apodemus* OTU, scaled twofold relative to the grand mean, are shown alongside the UPGMA phenogram.**Figure 7.** Co-phylogenetic comparison between the MSC phylogeny (left)

and the UPGMA phenogram based on Procrustes distances among mean OTU cranial shapes (right). Horizontal red lines connect corresponding taxa across the two trees. Mean cranial shapes for each *Apodemus* OTU, scaled twofold relative to the grand mean, are shown alongside the UPGMA phenogram.**Figure 8.** Co-phylogenetic comparison between the MSC phylogeny (left) and the UPGMA phenogram based on Procrustes distances among mean OTU molar shapes (right). Horizontal red lines connect corresponding taxa across the two trees. Mean molar shapes for each *Apodemus* OTU, scaled twofold relative to the grand mean, are shown alongside the UPGMA phenogram.

SUPPORTING INFORMATION

Supplementary material S1. Excel file provides a list of mitochondrial cytochrome *b* sequences obtained from GenBank and used in this study to reconstruct the maximum likelihood phylogenies of *Apodemus flavicollis* (Sheet 1) and *Apodemus uralensis* (Sheet 2). In both sheets, the "accession" column lists the GenBank accession numbers used to retrieve each sequence. The "organism" column indicates the species name as recorded in GenBank. The "geo_loc" column specifies the geographic origin of the sample, while "seq_len" gives the length of the sequence in base pairs. In the flavicollis sheet, the "genetic_lineage" column assigns each sequence to a genetic lineage (e.g., European or Middle Eastern) based on its phylogenetic placement in this study. The "reference" column provides the citation for the original study that published the sequence, where available. The uralensis sheet contains the same structure, but lacks the “genetic_lineage” column, reflecting the lack of geographic structuring in the genetic data for this species.

Supplementary material S2. Excel file provides detailed information on sequences used in the multispecies multilocus coalescent analysis (MSC) in this study. File is organized into three sheets: sequences, sample structure by gene, and reference list. The sequences sheet contains metadata for all specimens analysed. The "Taxon" column lists the species identification of each sample, while the "os" column indicates whether the species is represented in our morphometric dataset (yes/no). The column "used_in_phylogenetic_analysis" specifies whether the sample was included in the final MSC phylogenetic reconstruction. The following columns "cyt b", "IRBP", "RAG1", "I7", "vWF", "12S rRNA", "D-loop", and "COI" contain GenBank accession numbers for each gene, or “-” if the sequence is missing. The column "missing (%)" shows the percentage of missing loci per specimen. "Specimen" and "isolate" refer to individual sample identifiers,

while "origin" provides information on the geographic origin of the sample. The "reference" column lists numeric codes corresponding to the source of each sequence, as detailed in the reference list sheet. Additional sample-specific information is provided in the "comment" column. The sample structure by gene sheet summarizes the completeness of genetic data across all loci. For each gene, it reports the total number of individuals with available sequence data (both as absolute count and percentage out of 54), as well as the number and percentage of individuals for which data are missing. The reference list sheet contains full bibliographic citations corresponding to the numeric codes used in the "reference" column of the sequences sheet.

Supplementary Table S1. Pairwise post-hoc tests of size differences between *Apodemus* OTUs for mandible (Ma), cranium (Cr), and upper molars (Mo). R square (*Rsq*) and corresponding *P* values are given above and below the diagonal, respectively. Marked differences are significant ($P<0.001$ after Bonferroni correction).

Supplementary Table S2. Pairwise post-hoc tests of shape differences between *Apodemus* OTUs for mandible (Ma), cranium (Cr), and upper molars (Mo). R square (*Rsq*) and corresponding *P* values are given above and below the diagonal, respectively. Marked differences are significant ($P<0.001$ after Bonferroni correction).

Supplementary Figure S1. Phylogenetic relationships among 333 cytochrome *b* sequences of *Apodemus flavicollis* sensu lato, *A. ponticus*, *A. witherbyi* (reported as *A. fulvipectus*), and *A. sylvaticus* were reconstructed using a maximum likelihood approach implemented in IQ-TREE. Each sequence name follows the pattern: reported-species-name_location_accession-number. For example, af_Israel-Mt.Carmel_AJ605690 indicates: af, the GenBank-reported species (af = *Apodemus flavicollis*), followed by the sampling locality (Israel–Mt. Carmel), and the GenBank

accession number (AJ605690). Two divergent clades within *Apodemus flavicollis* sensu lato are highlighted based on their geographic distribution of sequences. *A. ponticus* corresponds to the Anatolian and Levantine samples of *A. flavicollis.* Red arrows mark sequences sampled from regions geographically proximate to our morphological dataset.

Supplementary Figure S2. Phylogenetic relationships among 132 cytochrome *b* sequences of *Apodemus uralensis* and *A. sylvaticus* were reconstructed using a maximum likelihood approach implemented in IQ-TREE. Each sequence name follows the pattern: reported-species-name_location_accession-number. For example, au_Czech.Republic-Moravia_AJ311154 indicates: au, the GenBank-reported species (au = *Apodemus uralensis*), followed by the sampling locality (Czech Republic–Moravia), and the GenBank accession number (AJ311154). No clear phylogeographic structure was observed within *A. uralensis*. Red arrows mark sequences sampled from regions geographically proximate to our morphological dataset.

Supplementary Figure S3. Plot of mean values of centroid size, standard deviations, and standard errors for the analysed *Apodemus* OTUs for mandible (A), cranium (B), and upper molars (C).

Supplementary Figure S4. Phylo-PCA plot of mean shapes for the analysed *Apodemus* OTUs for mandible (A), cranium (B), and upper molars (C).

HYSTRIX
the Italian Journal of Mammalogy

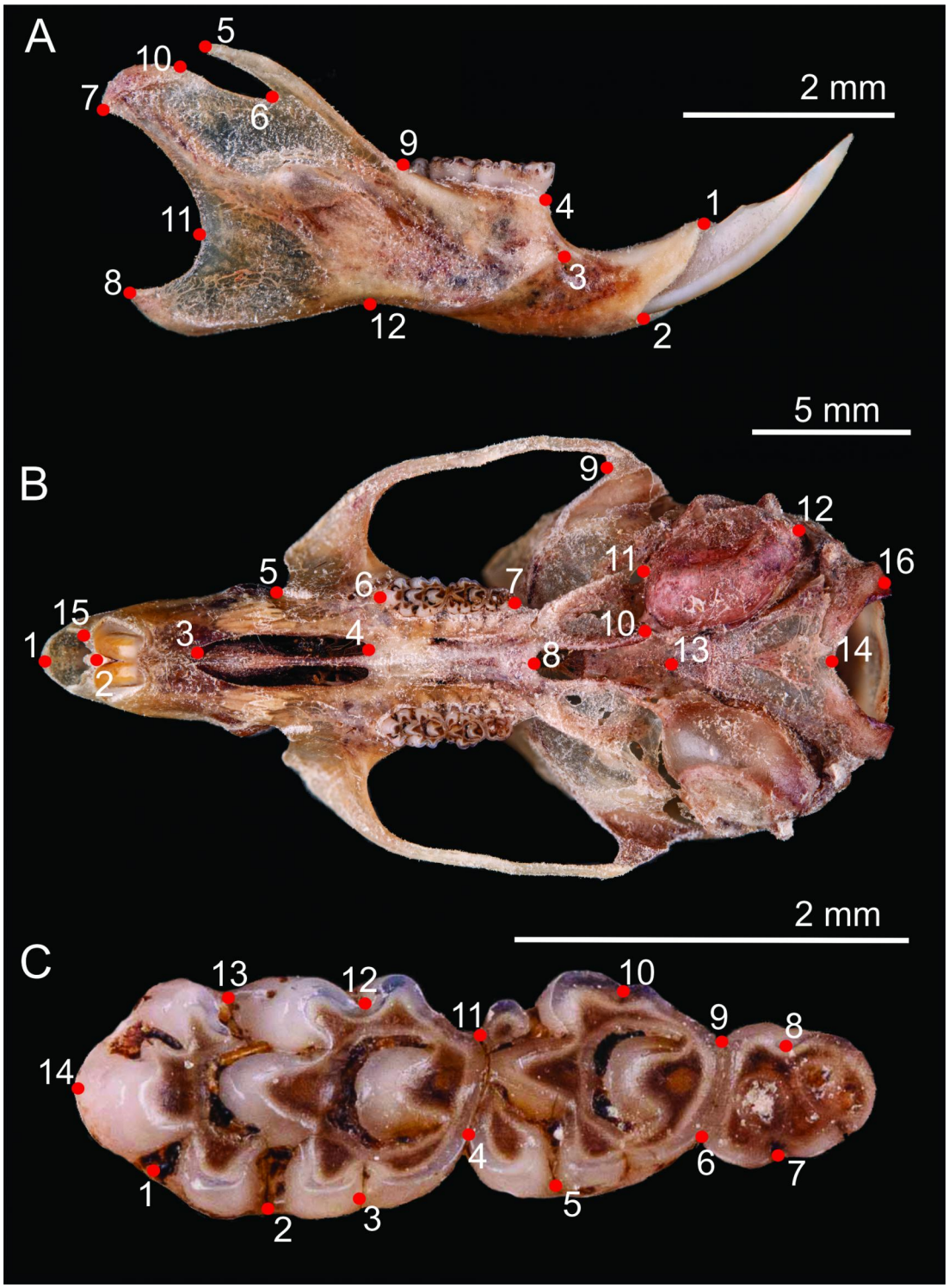

Figure 1. Landmarks collected on images of the mandible in labial view (A), cranium in ventral view (B), and upper molars in occlusal view (C).

HYSTRIX
the Italian Journal of Mammalogy

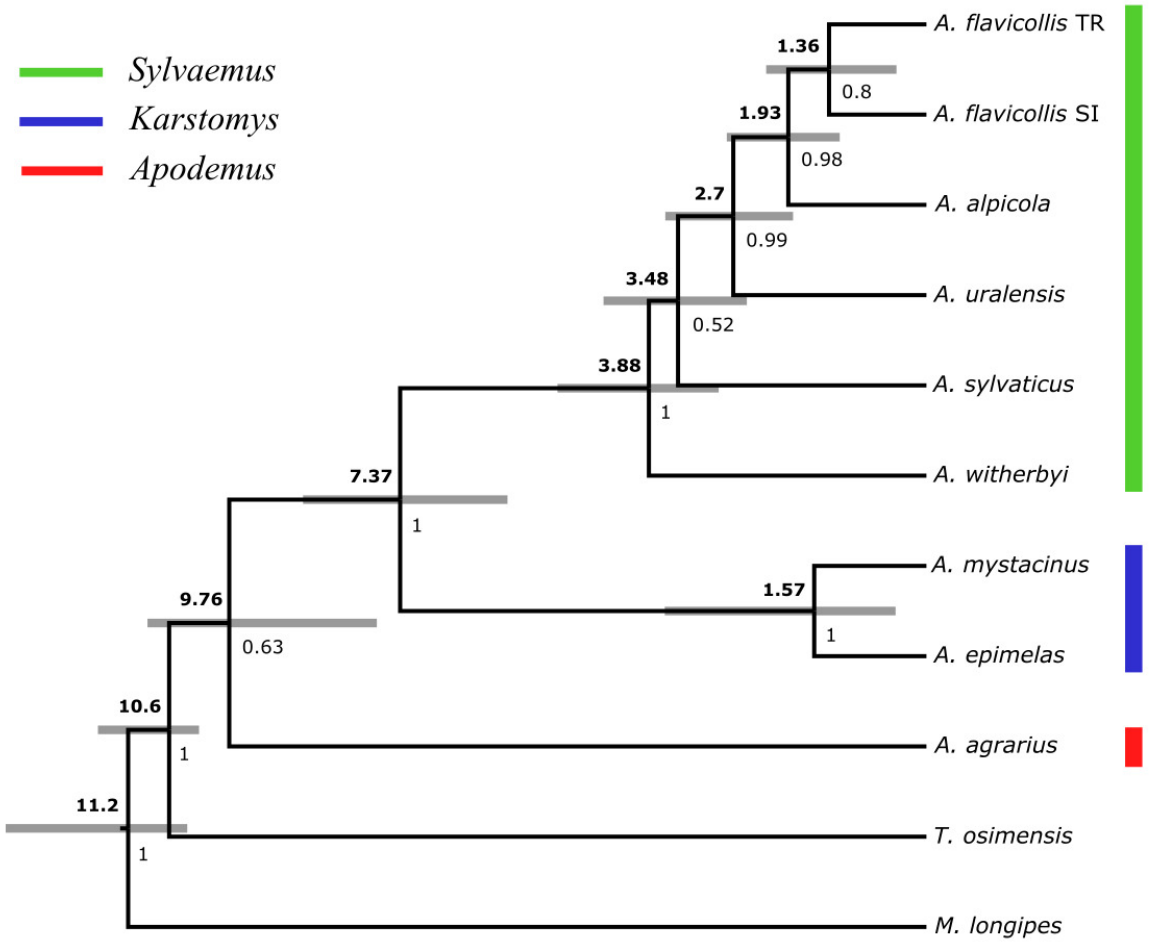

Figure 2. The maximum clade credibility phylogenetic relationship of a tribus Apodemini from the Western Palearctic inferred by Bayesian multispecies multilocus coalescent analyses in BEAST 2. Apodemini MRCA calibration point of about 10.7 Myr was used after Kimura et al. (2017). Node bars indicate the 95% credible interval of the posterior density of divergence times which is expressed in millions of years (Myr) ago since presence. The posterior median of divergence times are in bold, depicted on the left-hand side of each node, while posterior support for node splits are on the right-hand side of each node. Apodemus subgenera are colored as: Sylvaemus (green), Karstomys (blue) and Apodemus (red).

HYSTRIX
the Italian Journal of Mammalogy

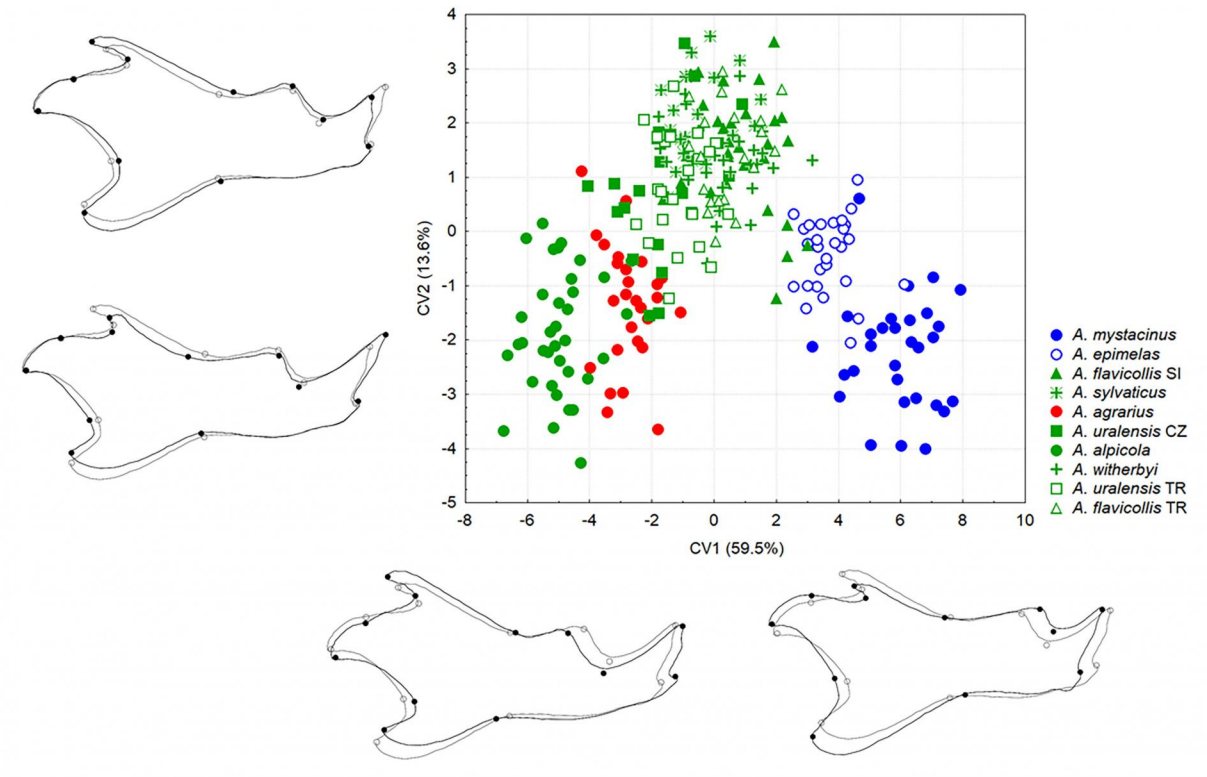

Figure 3. CVA scatterplots of the first and second CV axes for the mandible. Shape changes along CV axes are visualized by warped outline drawings that are magnified two times.

HYSTRIX
the Italian Journal of Mammalogy

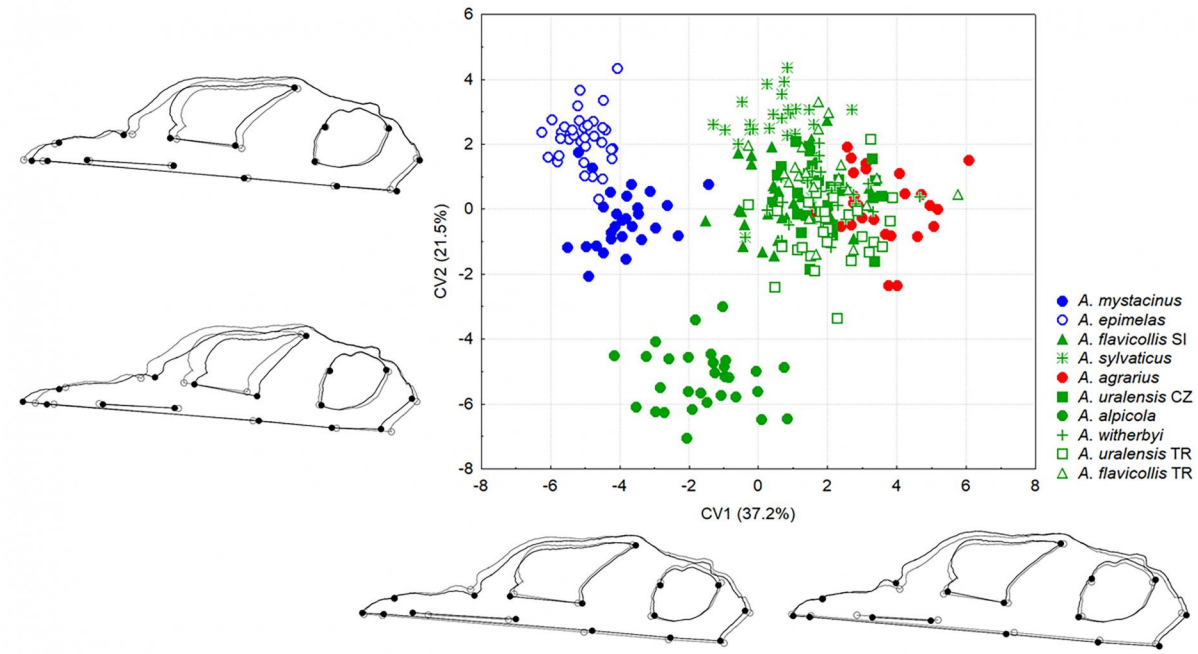

Figure 4. CVA scatterplots of the first and second CV axes for the cranium. Shape changes along CV axes are visualized by warped outline drawings that are magnified two times.

HYSTRIX
the Italian Journal of Mammalogy

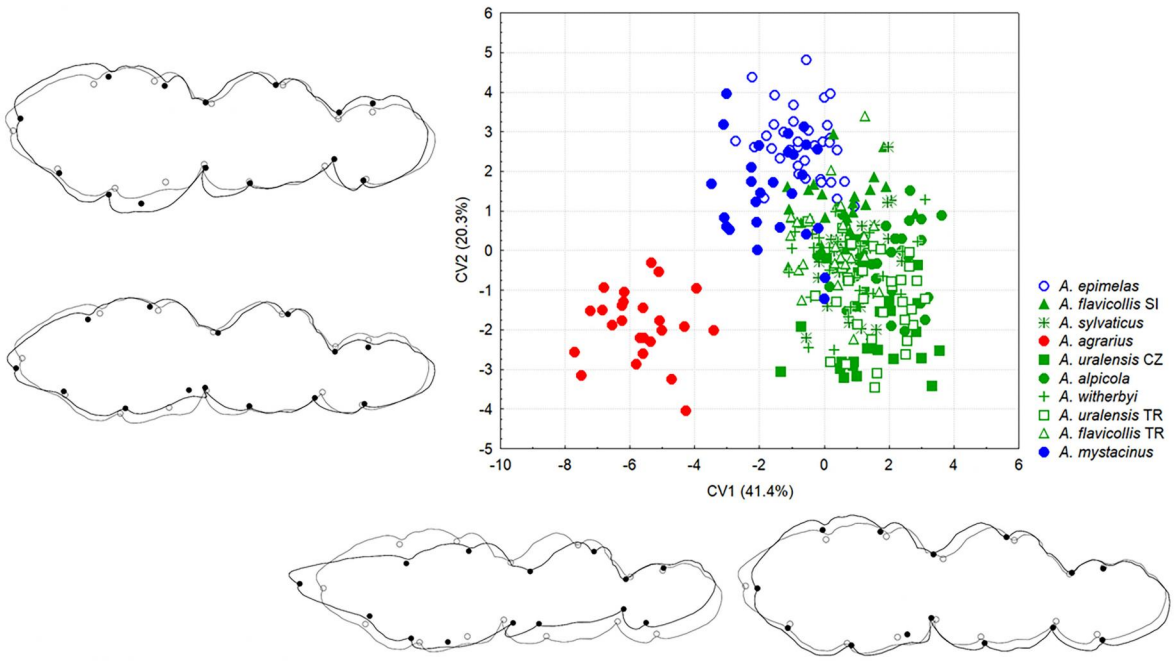

Figure 5. CVA scatterplots of the first and second CV axes for upper molars. Shape changes along CV axes are visualized by warped outline drawings that are magnified two times.

HYSTRIX
the Italian Journal of Mammalogy

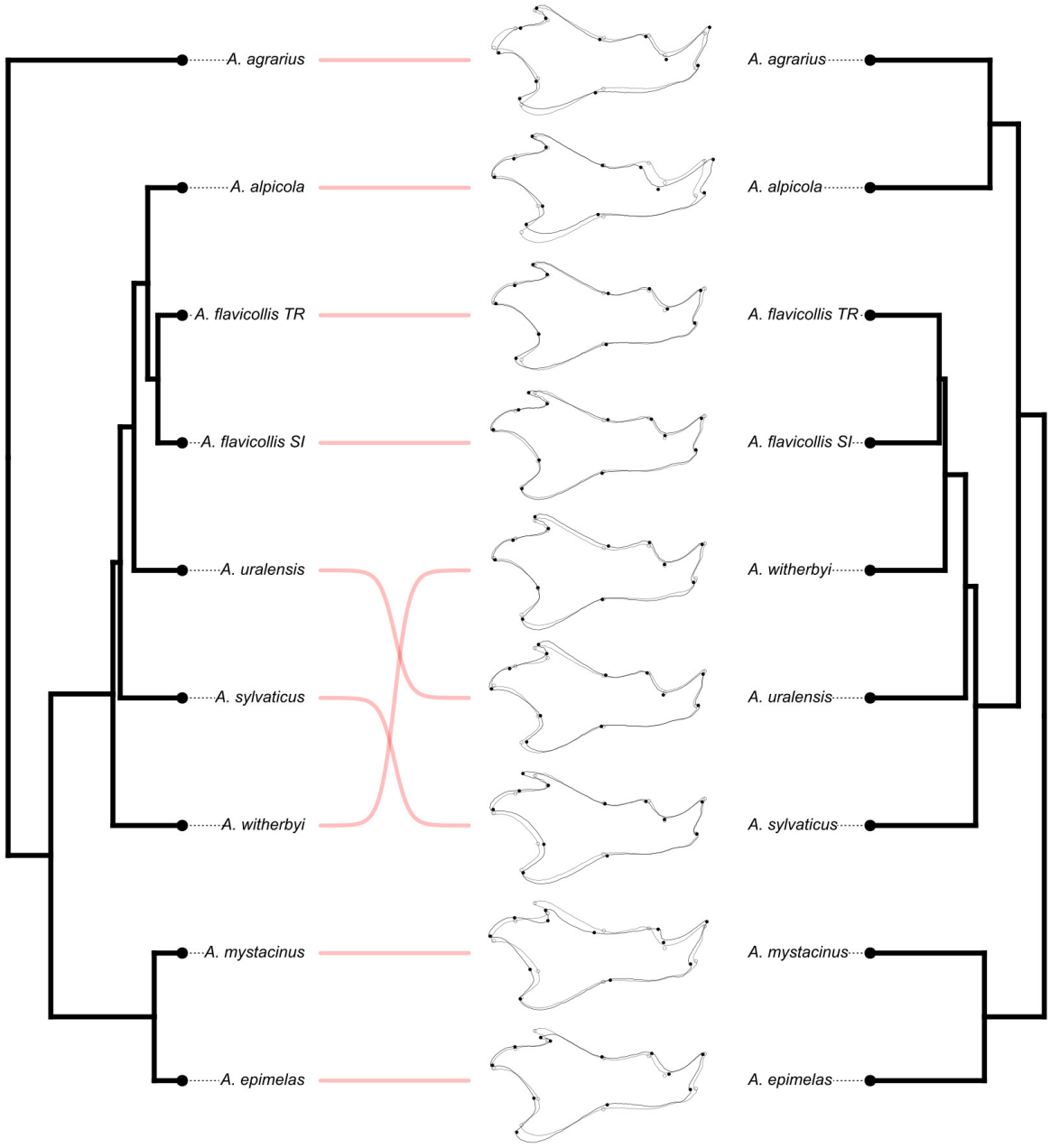

Figure 6. Co-phylogenetic comparison between the MSC phylogeny (left) and the UPGMA phenogram based on Procrustes distances among mean OTU mandibular shapes (right). Horizontal red lines connect corresponding taxa across the two trees. Mean mandibular shapes for each Apodemus OTU, scaled twofold relative to the grand mean, are shown alongside the UPGMA phenogram.

HYSTRIX
the Italian Journal of Mammalogy

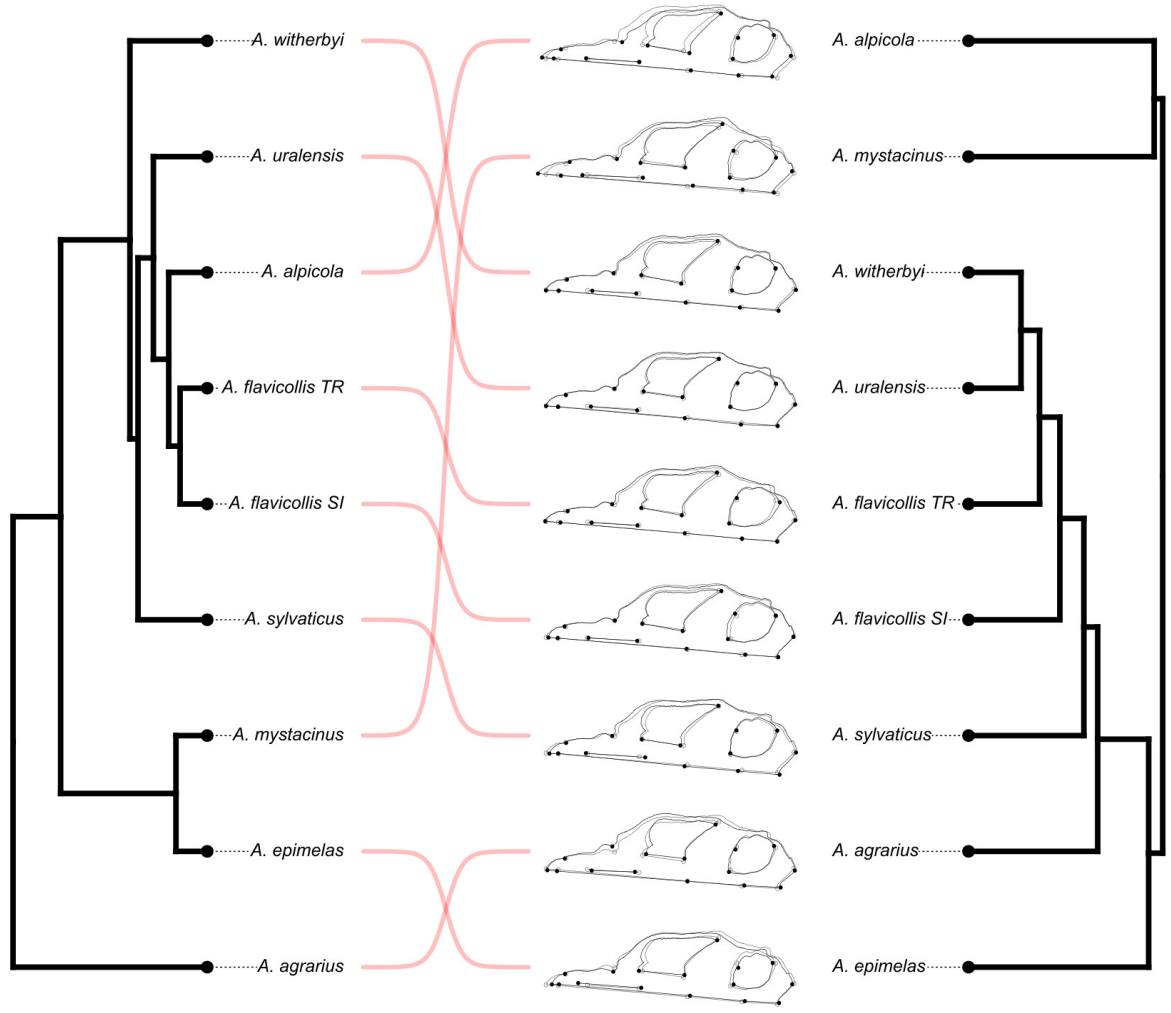

Figure 7. Co-phylogenetic comparison between the MSC phylogeny (left) and the UPGMA phenogram based on Procrustes distances among mean OTU cranial shapes (right). Horizontal red lines connect corresponding taxa across the two trees. Mean cranial shapes for each Apodemus OTU, scaled twofold relative to the grand mean, are shown alongside the UPGMA phenogram.

HYSTRIX
the Italian Journal of Mammalogy

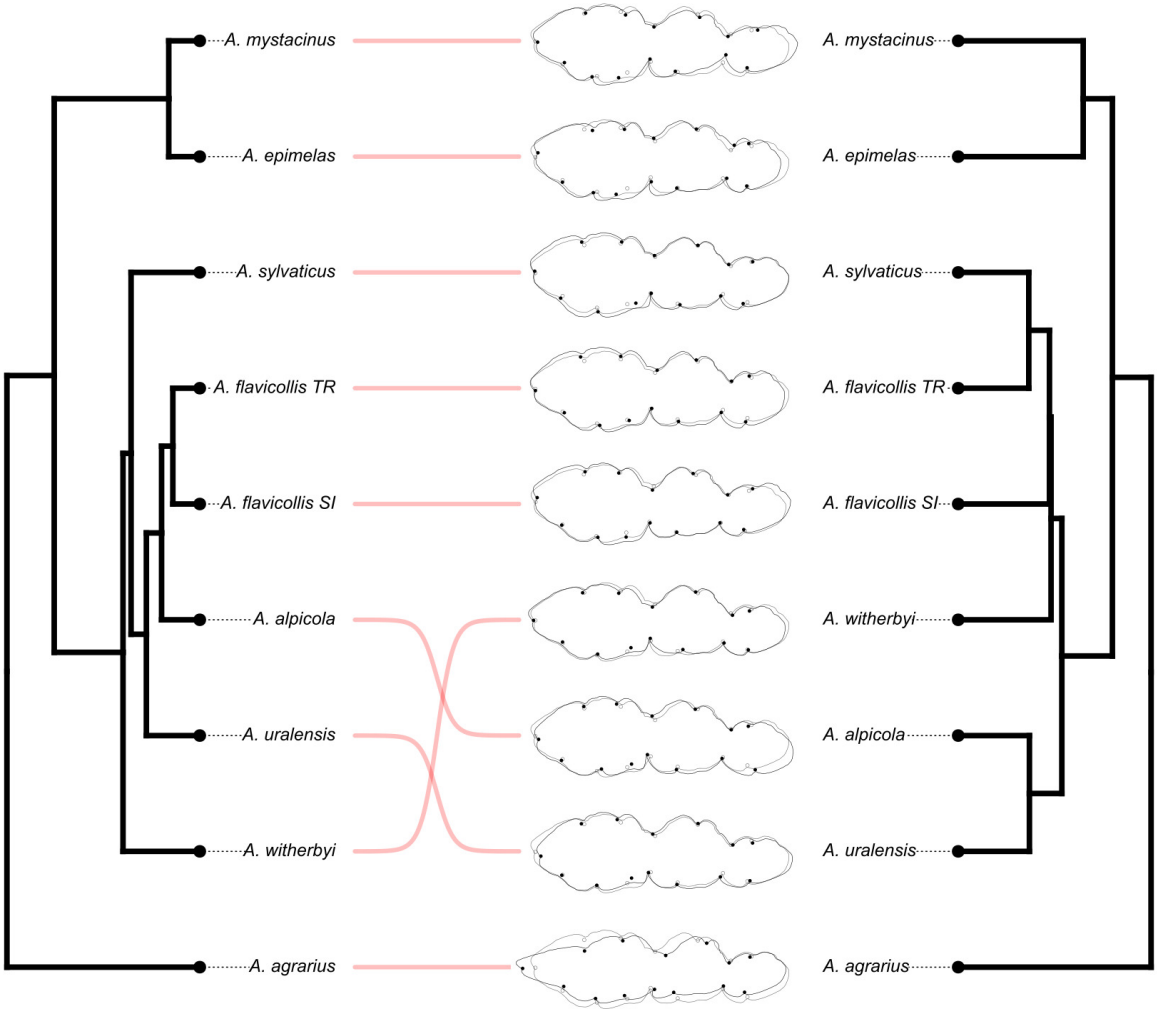

Figure 8. Co-phylogenetic comparison between the MSC phylogeny (left) and the UPGMA phenogram based on Procrustes distances among mean OTU molar shapes (right). Horizontal red lines connect corresponding taxa across the two trees. Mean molar shapes for each Apodemus OTU, scaled twofold relative to the grand mean, are shown alongside the UPGMA phenogram.

Manuscript body

Download source file (110.65 kB)

Figures

Figure 1 - Download source file (6.9 MB)
Figure 1. Landmarks collected on images of the mandible in labial view (A), cranium in ventral view (B), and upper molars in occlusal view (C).

Figure 2 - Download source file (78.84 kB)
Figure 2. The maximum clade credibility phylogenetic relationship of a tribus Apodemini from the Western Palearctic inferred by Bayesian multispecies multilocus coalescent analyses in BEAST 2. Apodemini MRCA calibration point of about 10.7 Myr was used after Kimura et al. (2017). Node bars indicate the 95% credible interval of the posterior density of divergence times which is expressed in millions of years (Myr) ago since presence. The posterior median of divergence times are in bold, depicted on the left-hand side of each node, while posterior support for node splits are on the right-hand side of each node. Apodemus subgenera are colored as: Sylvaemus (green), Karstomys (blue) and Apodemus (red).

Figure 3 - Download source file (1.49 MB)
Figure 3. CVA scatterplots of the first and second CV axes for the mandible. Shape changes along CV axes are visualized by warped outline drawings that are magnified two times.

Figure 4 - Download source file (1.71 MB)
Figure 4. CVA scatterplots of the first and second CV axes for the cranium. Shape changes along CV axes are visualized by warped outline drawings that are magnified two times.

Figure 5 - Download source file (1.61 MB)
Figure 5. CVA scatterplots of the first and second CV axes for upper molars. Shape changes along CV axes are visualized by warped outline drawings that are magnified two times.

Figure 6 - Download source file (258.6 kB)
Figure 6. Co-phylogenetic comparison between the MSC phylogeny (left) and the UPGMA phenogram based on Procrustes distances among mean OTU mandibular shapes (right). Horizontal red lines connect corresponding taxa across the two trees. Mean mandibular shapes for each Apodemus OTU, scaled twofold relative to the grand mean, are shown alongside the UPGMA phenogram.

Figure 7 - Download source file (289.46 kB)
Figure 7. Co-phylogenetic comparison between the MSC phylogeny (left) and the UPGMA phenogram based on Procrustes distances among mean OTU cranial shapes (right). Horizontal red lines connect corresponding taxa across the two trees. Mean cranial shapes for each Apodemus OTU, scaled twofold relative to the grand mean, are shown alongside the UPGMA phenogram.

Figure 8 - Download source file (251.65 kB)
Figure 8. Co-phylogenetic comparison between the MSC phylogeny (left) and the UPGMA phenogram based on Procrustes distances among mean OTU molar shapes (right). Horizontal red lines connect corresponding taxa across the two trees. Mean molar shapes for each Apodemus OTU, scaled twofold relative to the grand mean, are shown alongside the UPGMA phenogram.

Supplementary Online Material

File 1 - Download source file (33.44 kB)
Supplementary material S1. Excel file provides a list of mitochondrial cytochrome b sequences obtained from GenBank and used in this study to reconstruct the maximum likelihood phylogenies of Apodemus flavicollis (Sheet 1) and Apodemus uralensis (Sheet

2). In both sheets, the "accession" column lists the GenBank accession numbers used to retrieve each sequence. The "organism" column indicates the species name as recorded in GenBank. The "geo_loc" column specifies the geographic origin of the sample, while "seq_len" gives the length of the sequence in base pairs. In the flavicollis sheet, the "genetic_lineage" column assigns each sequence to a genetic lineage (e.g., European or Middle Eastern) based on its phylogenetic placement in this study. The "reference" column provides the citation for the original study that published the sequence, where available. The uralensis sheet contains the same structure, but lacks the “genetic_lineage” column, reflecting the lack of geographic structuring in the genetic data for this species.

File 2 - Download source file (22.15 kB)
Supplementary material S2. Excel file provides detailed information on sequences used in the multispecies multilocus coalescent analysis (MSC) in this study. File is organized into three sheets: sequences, sample structure by gene, and reference list. The sequences sheet contains metadata for all specimens analyzed. The "Taxon" column lists the species identification of each sample, while the "os" column indicates whether the species is represented in our morphometric dataset (yes/no). The column "used_in_phylogenetic_analysis" specifies whether the sample was included in the final MSC phylogenetic reconstruction. The following columns "cyt b", "IRBP", "RAG1", "I7", "vWF", "12S rRNA", "D-loop", and "COI" contain GenBank accession numbers for each gene, or “-” if the sequence is missing. The column "missing (%)" shows the percentage of missing loci per specimen. "Specimen" and "isolate" refer to individual sample identifiers, while "origin" provides information on the geographic origin of the sample. The "reference" column lists numeric codes corresponding to the source of each sequence, as detailed in the reference list sheet. Additional sample-specific information is provided in the "comment" column. The sample structure by gene sheet summarizes the completeness of genetic data across all loci. For each gene, it reports the total number of individuals with available sequence data (both as absolute count and percentage out of 54), as well as the number and percentage of individuals for which data are missing. The reference list sheet contains full bibliographic citations corresponding to the numeric codes used in the "reference" column of the sequences sheet.

File 3 - Download source file (19.33 kB)
Supplementary Table S1. Pairwise post-hoc tests of size differences between Apodemus OTUs for mandible (Ma), cranium (Cr), and upper molars (Mo). R square (Rsq) and corresponding P values are given above and below the diagonal, respectively. Marked differences are significant (P<0.001 after Bonferroni correction).

File 4 - Download source file (19.22 kB)
Supplementary Table S2. Pairwise post-hoc tests of shape differences between Apodemus OTUs for mandible (Ma), cranium (Cr), and upper molars (Mo). R square (Rsq) and corresponding P values are given above and below the diagonal, respectively. Marked differences are significant (P<0.001 after Bonferroni correction).

File 5 - Download source file (5.66 MB)
Supplementary Figure S1. Phylogenetic relationships among 333 cytochrome b sequences of Apodemus flavicollis sensu lato, A. ponticus, A. witherbyi (reported as A. fulvipectus), and A. sylvaticus were reconstructed using a maximum likelihood approach implemented in IQ-TREE. Each sequence name follows the pattern: reported-species-name_location_accession-number. For example, af_Israel-Mt.Carmel_AJ605690 indicates: af, the GenBank-reported species (af = Apodemus flavicollis), followed by the sampling locality (Israel–Mt. Carmel), and the GenBank accession number (AJ605690). Two divergent clades within Apodemus flavicollis sensu lato are highlighted based on their geographic distribution of sequences. A. ponticus corresponds to the Anatolian and Levantine samples of A. flavicollis. Red arrows mark sequences sampled from regions geographically proximate to our morphological dataset.

File 6 - Download source file (3.26 MB)

Supplementary Figure S2. Phylogenetic relationships among 132 cytochrome b sequences of Apodemus uralensis and A. sylvaticus were reconstructed using a maximum likelihood approach implemented in IQ-TREE. Each sequence name follows the pattern: reported-species-name_location_accession-number. For example, au_Czech.Republic-Moravia_AJ311154 indicates: au, the GenBank-reported species (au = Apodemus uralensis), followed by the sampling locality (Czech Republic–Moravia), and the GenBank accession number (AJ311154). No clear phylogeographic structure was observed within A. uralensis. Red arrows mark sequences sampled from regions geographically proximate to our morphological dataset.

File 7 - Download source file (123.32 kB)
Supplementary Figure S3. Plot of mean values of centroid size, standard deviations, and standard errors for the analysed Apodemus OTUs for mandible (A), cranium (B), and upper molars (C).

File 8 - Download source file (835.46 kB)
Supplementary Figure S4. Phylo-PCA plot of mean shapes for the analysed Apodemus OTUs for mandible (A), cranium (B), and upper molars (C).